Materials Today Bio 29 (2024) 101353

Contents lists available at ScienceDirect

Materials Today Bio

journal homepage: www.journals.elsevier.com/materials-today-bio

Enhanced therapeutic potential of a self-healing hyaluronic acid hydrogel for early intervention in osteoarthritis

Dongze Wu [a,1], Shuhui Yang [c,1], Zhe Gong [b], Xinxin Zhu [e], Juncong Hong [f], Haitao Wang [b], Wenbin Xu [b], Juncheng Lai [c], Xiumei Wang [d], Jiye Lu [a], Xiangqian Fang [b,**], Guoqiang Jiang [a,***], Jinjin Zhu [b,*]

[a] Department of Spinal Surgery, The First Affiliated Hospital of Ningbo University, Ningbo, 315000, Zhejiang, China
[b] Department of Orthopedic Surgery, Sir Run Run Shaw Hospital, Zhejiang University School of Medicine & Zhejiang Key Laboratory of Mechanism Research and Precision Repair of Orthopaedic Trauma and Aging Diseases, Hangzhou, 310016, Zhejiang, China
[c] School of Materials Science and Engineering, Zhejiang-Mauritius Joint Research Center for Biomaterials and Tissue Engineering, Zhejiang Sci-Tech University, Hangzhou, 310018, Zhejiang, China
[d] State Key Laboratory of New Ceramics and Fine Processing, Key Laboratory of Advanced Materials, School of Materials Science and Engineering, Tsinghua University, Beijing, 100084, China
[e] Stomatology Hospital, School of Stomatology, Zhejiang University School of Medicine, Zhejiang Provincial Clinical Research Center for Oral Diseases, Key Laboratory of Oral Biomedical Research of Zhejiang Province, Cancer Center of Zhejiang University, Engineering Research Center of Oral Biomaterials and Devices of Zhejiang Province, Hangzhou, 310000, Zhejiang, China
[f] Department of Anesthesiology, The First People's Hospital of Linping District, Hangzhou, 311100, Zhejiang, China

ARTICLE INFO

Keywords:
Osteoarthritis
Hyaluronic acid hydrogel
Self-healing
Injectability
Cartilage surface friction

ABSTRACT

Osteoarthritis (OA) is characterized by symptoms such as abnormal lubrication function of synovial fluid and heightened friction on the cartilage surface in its early stages, prior to evident cartilage damage. Current early intervention strategies employing lubricated hydrogels to shield cartilage from friction often overlook the significance of hydrogel-cartilage adhesion and enhancement of the cartilage extracellular matrix (ECM). Herein, we constructed a hydrogel based on dihydrazide-modified hyaluronic acid (HA) (AHA) and catechol-conjugated aldehyde-modified HA (CHA), which not only adheres to the cartilage surface as an effective lubricant but also improves the extracellular environment of chondrocytes in OA. Material characterization experiments on AHA/CHA hydrogels with varying concentrations validated their exceptional self-healing capabilities, superior injectability and viscoelasticity, sustained adhesion strength to cartilage, and a low friction coefficient. Chondrocytes exhibited robust adhesion and proliferation on the AHA/CHA hydrogel surface, with the upregulation of cartilage matrix protein expression. Intra-articular injection of AHA/CHA hydrogels was performed following destabilization of the medial meniscus (DMM) surgery in mice to assess its protective effect on cartilage. The AHA/CHA hydrogel effectively attenuated the degree of cartilage wear, facilitated chondrocytes' anabolic metabolism, and restored the ECM of cartilage. Therefore, the AHA/CHA hydrogel emerges as a promising therapeutic approach in clinical practices of OA treatment.

1. Introduction

Osteoarthritis, a prevalent type of arthritis, impacts 27 million individuals in the United States and is associated with an estimated annual medical cost of $185 billion [1]. OA is a complex process involving joint overload, wear, metabolic disorders, and inflammation [2]. Early OA is characterized by reduced HA content in the synovial fluid of the joint, leading to cartilage wear after impaired joint lubrication [3]. Cartilage wear leads to activation of signaling pathways, which produce a series of catabolic enzymes that degrade the functional cartilage extracellular

* Corresponding author.
** Corresponding author.
*** Corresponding author.
E-mail addresses: orthofxq@zju.edu.cn (X. Fang), jiangguoqiang@nbu.edu.cn (G. Jiang), zjjspine003@zju.edu.cn (J. Zhu).
[1] These authors contributed equally to this work.

https://doi.org/10.1016/j.mtbio.2024.101353
Received 23 May 2024; Received in revised form 9 November 2024; Accepted 18 November 2024
Available online 21 November 2024

matrix [4]. In the late stage of OA, the complete wear and destruction of articular cartilage inevitably causes joint stiffness and disability [5]. The degradation of cartilage caused by OA is a gradual and progressive process. Timely intervention and treatment can potentially impede or delay the advancement of OA, thereby preventing irreversible damage to the affected joint cartilage [6]. Therefore, early intervention for patients with OA, such as supplementation of synovial fluid, proves highly effective and imperative [7].

Synovial fluid is a natural lubricant between articular cartilage surfaces, capable of lubrication by elastic fluid dynamics, providing functions such as shock absorption, load support, and almost frictionless sliding motion [8]. Synovial fluid is a special ultrafiltrate of blood that is rich in hyaluronic acid and proteoglycan 4 [9]. HA plays a significant role in maintaining joint stability by providing synovial fluid with viscoelastic and lubricating properties. Intra-articular HA injection was considered effective in maintaining a low friction coefficient on the articular surface during early-stage OA before the onset of cartilage damage [10,11]. A variety of commercial HA joint lubricants have been used in clinical practice. However, HA lubricants exhibit inferior mechanical properties and undergo rapid degradation, thus requiring frequent intra-articular injections, which not only increases the susceptibility to infection and treatment costs but also deters patients from undergoing repeated injections due to their reluctance [12].

HA can form a lubricant hydrogel by physical or chemical means, which can effectively prolong its retention time in joints [13]. Lubricated hydrogels based on HA, leveraging its exceptional lubricating properties, have been extensively explored in osteoarthritis research [14]. However, HA hydrogels still face many problems. Lei et al. synthesized a 3-aminophenylboronic acid-modified HA and then cross-linked it with a hydroxyl group containing polyvinyl alcohol to construct an injectable, self-healing lubricating hydrogel. However, the potential side effects of polyvinyl alcohol cannot be disregarded [15]. Cai et al. synthesized lubricating hydrogels consisting of vinyl-modified HA and dithiol functionalized poly(ethylene glycol). However, poor injectability limits its intra-articular applications [14]. Chen et al. introduced a chemically modified gellan gum-HA hydrogel, resistant to enzymatic degradation and extending its joint residence time; however, it only acts as a pure mucus supplement without the adhesive properties [16].

The adhesive properties of hydrogels enhance the therapeutic effects on OA. Adhesive HA hydrogels are commonly used for cartilage regeneration, owing to the advantage of mimicking the chondrocyte-like extracellular matrix environment and promoting the chondrogenic differentiation of stem cells. Chen et al. prepared an aldehyde and methacrylate-modified injectable adhesive HA hydrogel that significantly improved cartilage regeneration in a rat osteochondral defect model [17]. The glycosaminoglycan hydrogel developed by Bordbar et al. exhibited the potential to enhance cell adhesion and create a conducive microenvironment for cellular activities, thereby offering promising prospects for its application in OA [18]. However, lubricating

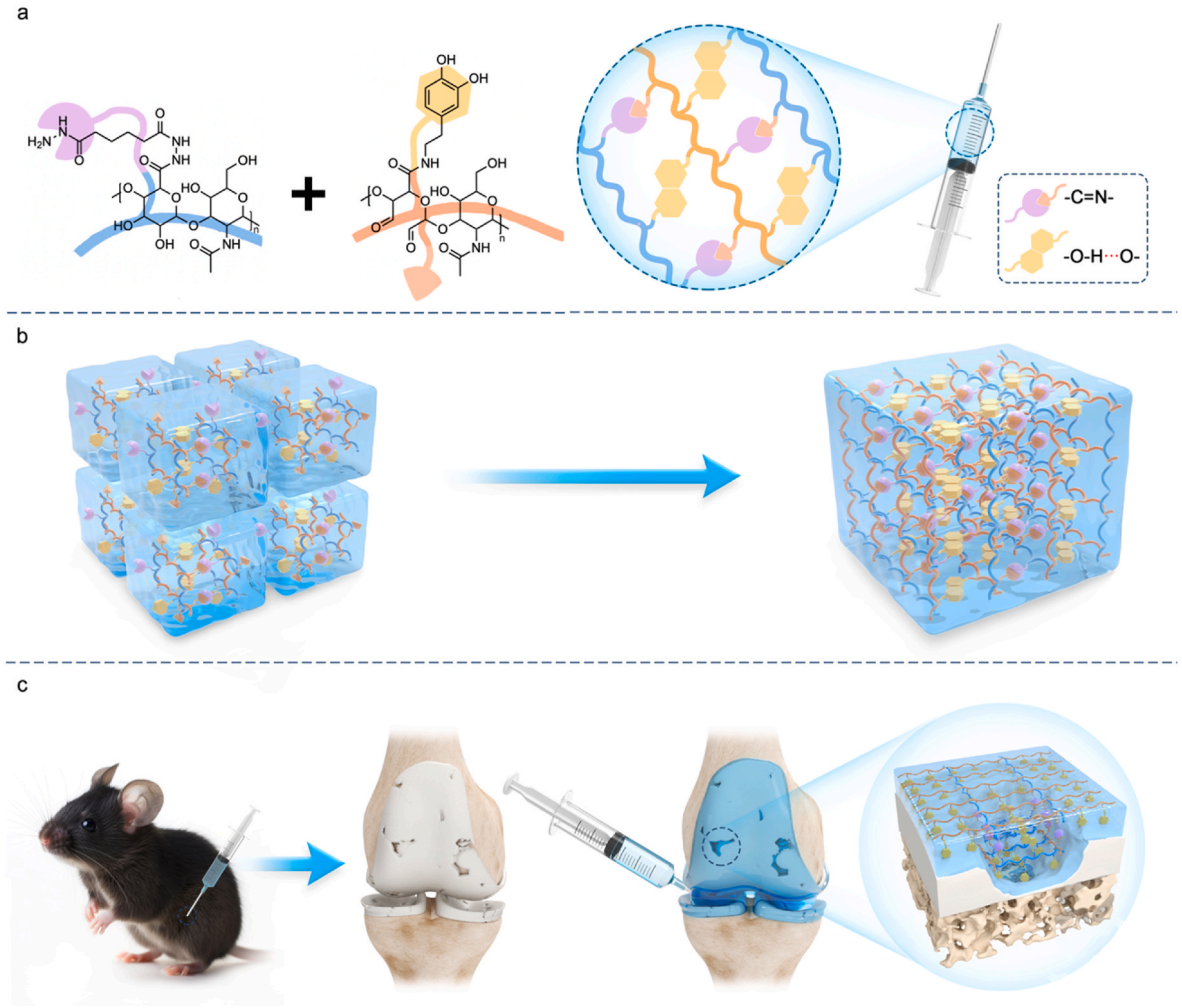

Fig. 1. Illustration of the structure and functional characteristics of AHA/CHA hydrogels. a) AHA/CHA hydrogels rely on Schiff base cross-linking for gelation, and contain abundant hydrogen bonds. b) The fragmented AHA/CHA hydrogel can quickly self-healing. c) The AHA/CHA hydrogel has excellent injectability and adhesion to cartilage.

hydrogels seldom exhibit adhesive properties, and most of the studies on lubricated hydrogels disregard the interaction between the cartilage surface and the lubricant. Thus, the ideal hydrogel lubricant should possess good injectability and biocompatibility, as well as superior lubrication and adhesive capabilities to enhance the protection of cartilage.

We previously developed a self-assembling peptide hydrogel as a carrier for microRNA delivery to supplement synovial fluid and demonstrated that it effectively delayed OA progression in mice [19]. Considering the preventive effect of lubrication in the early stages of OA, we aim to develop a novel HA-based adhesive hydrogel lubrication strategy. In this study, we developed a simple and effective self-healing HA lubricant hydrogel by binding dopamine to increase its adhesion capabilities (Fig. 1a and b). The structural composition, physical properties, and application of AHA/CHA hydrogels in cell culture in vitro were thoroughly examined. Subsequently, we evaluated the effect of the AHA/CHA hydrogels in mitigating cartilage wear in OA mice (Fig. 1c) To gain further insights into the mechanism by which AHA/CHA hydrogels influence chondrocytes and potentially inhibit OA development, we employed RNA sequencing to validate potential signaling pathways that may be modulated by the hydrogel, thereby shedding light on its therapeutic potential.

2. Results

2.1. Properties of AHA/CHA hydrogels

^{1}H nuclear magnetic resonance (NMR) (Fig. 2a) and Fourier transform infrared (FTIR) (Fig. 2b) spectra were used to confirm the chemical formulas of HA and modified HA. The characteristic peak of AHA was identified at δ 1.65 ppm (-CH_2-CH_2-) [20] and 3200 cm^{-1} (-N-H) [21]. The grafting degree of AHA modification was determined to be 63.1 % by calculating the integral area ratio between δ 1.65 ppm and δ 3–4 ppm. In order to obtain CHA, HA was first oxidated by sodium periodate to open part of the backbone carbon ring and form an aldehyde group (OHA), with a grafting degree of 58.4 % indicated by hydroxylamine hydrochloride titration. Peaks representing the aldehyde groups were observed at δ 5 ppm and 1705 cm^{-1} [22]. Subsequently, CHA was synthesized by adding the catechol functional group to OHA, and the peak corresponding to the benzene ring was observed at 670 cm^{-1} and δ 2.8 ppm (-CH_2CH_2-). The grafting degree of catechol modification in CHA was determined to be 44.7 % by calculating the area ratio of δ 1.8

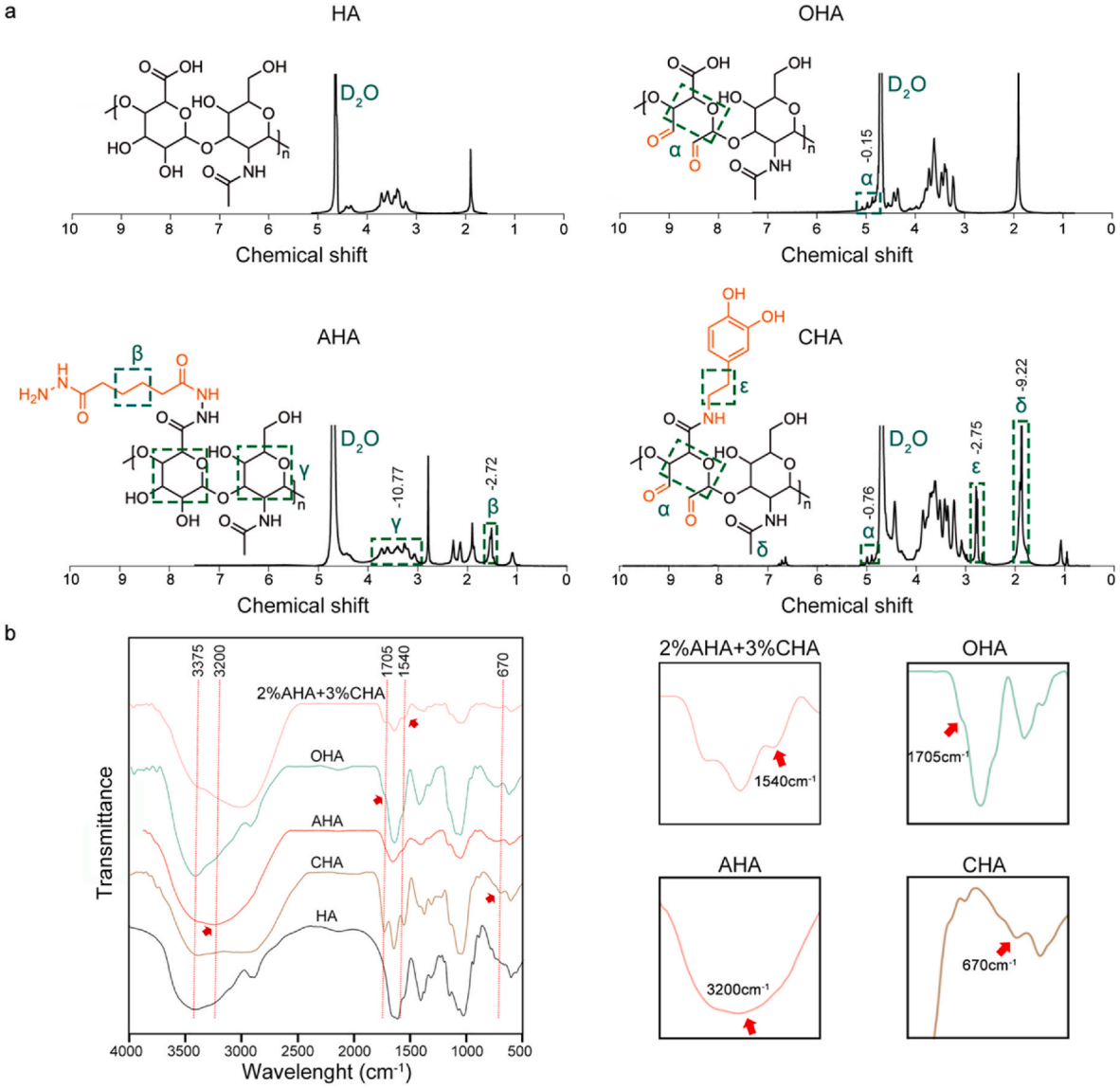

Fig. 2. Chemical characterization of modified-HA. a) ^{1}H NMR spectra of HA, AHA, OHA, and CHA. α: CH-CH-O-CH-. β: CH_2-CH_2-. γ: CH-CH-CH-CH-CH-. δ: CH_3. ε: CH_2-CH_2-. D_2O: deuterium oxide. b) FTIR spectra of AHA/CHA hydrogels, OHA, AHA, CHA and HA.

ppm (-CH_3) and δ 2.8 ppm. Furthermore, we observed that the characteristic vibrational peak of the amide bond (-C=N) appeared at 1540 cm^{-1} in the AHA/CHA hydrogel, indicating Schiff base formation [23]. These results demonstrated the successful modification of HA.

To prepare solutions of 2 % and 3 % AHA, 1 ml of deionized water was added to 20 mg and 30 mg of AHA, respectively. Similarly, solutions of 3 %, 4 %, and 5 % CHA were formulated using the identical method. Throughout this paper, all AHA and CHA solutions were uniformly mixed in a consistent 2:1 vol ratio.

After mixing 2 % AHA with 3 % CHA, the gelation process was completed in 1 min. Subsequently, when the glass bottle was inverted, it was noteworthy that the hydrogel remained stationary and adhered to the bottom of the bottle, resisting the gravitational force. This observation marked a distinct transition from the sol to the gel phase (Fig. 3a). The rapid self-healing capability of the 2 % AHA +3 % CHA hydrogel was further demonstrated. As illustrated in Fig. 3b and Video. S1, two differently colored segments of the AHA/CHA hydrogel seamlessly merged within 45 s after attachment. Notably, the intervening cracks vanished entirely, as evidenced in Fig. S1, showcasing the hydrogel's swift and efficient self-repair process.

The micromorphology of the AHA/CHA hydrogels was examined using a scanning electron microscope (SEM). As shown in Fig. 3c, the surface of AHA/CHA hydrogels contains abundant pores. The average pore diameters of the different AHA/CHA hydrogels measured from SEM images were 34.76 ± 5.67 μm, 48.45 ± 10.06 μm, 36.38 ± 2.37 μm, 65.63 ± 8.07 μm, 59.24 ± 10.89 μm, and 51.50 ± 4.40 μm. When the concentration of CHA was varied while maintaining a constant concentration of AHA, no significant difference in the average pore size of the hydrogel was observed, suggesting the structural integrity despite compositional adjustments (Fig. S2).

The rheological properties of different AHA/CHA hydrogels were also evaluated. The AHA/CHA hydrogel network collapsed and recovered under alternating strains of 1 % and 350 %, further indicating a rapid self-healing ability (Fig. 3d). In the time-sweep mode, G′ (storage modulus) was significantly higher than G″ (loss modulus), indicating the stabilization of the AHA/CHA hydrogel state (Fig. S3). In the strain-sweep mode, the G′ of the hydrogel remained stable when subjected to shear strain below 100 %, whereas it underwent a significant decline beyond 100 %, particularly approaching 1000 % strain, indicating that the AHA/CHA hydrogel possesses a broad linear viscoelastic region (Fig. 3e). Notably, the 2 % AHA +3 % CHA and 3 % AHA +3 % CHA hydrogels had the lowest G′, which was approximately 150 Pa.

The rapid decrease in viscosity as the shear rate increased indicated that the AHA/CHA hydrogels exhibited excellent injectability (Fig. 3f). In practice, both the AHA/CHA hydrogel (2 % AHA + 3 % CHA) and the commercial HA joint lubricant (ARTZ Dispo) could be effortlessly extruded through an insulin injection needle (29G) without obstruction (Fig. 3g). Remarkably, the hydrogel was extruded from the needle under

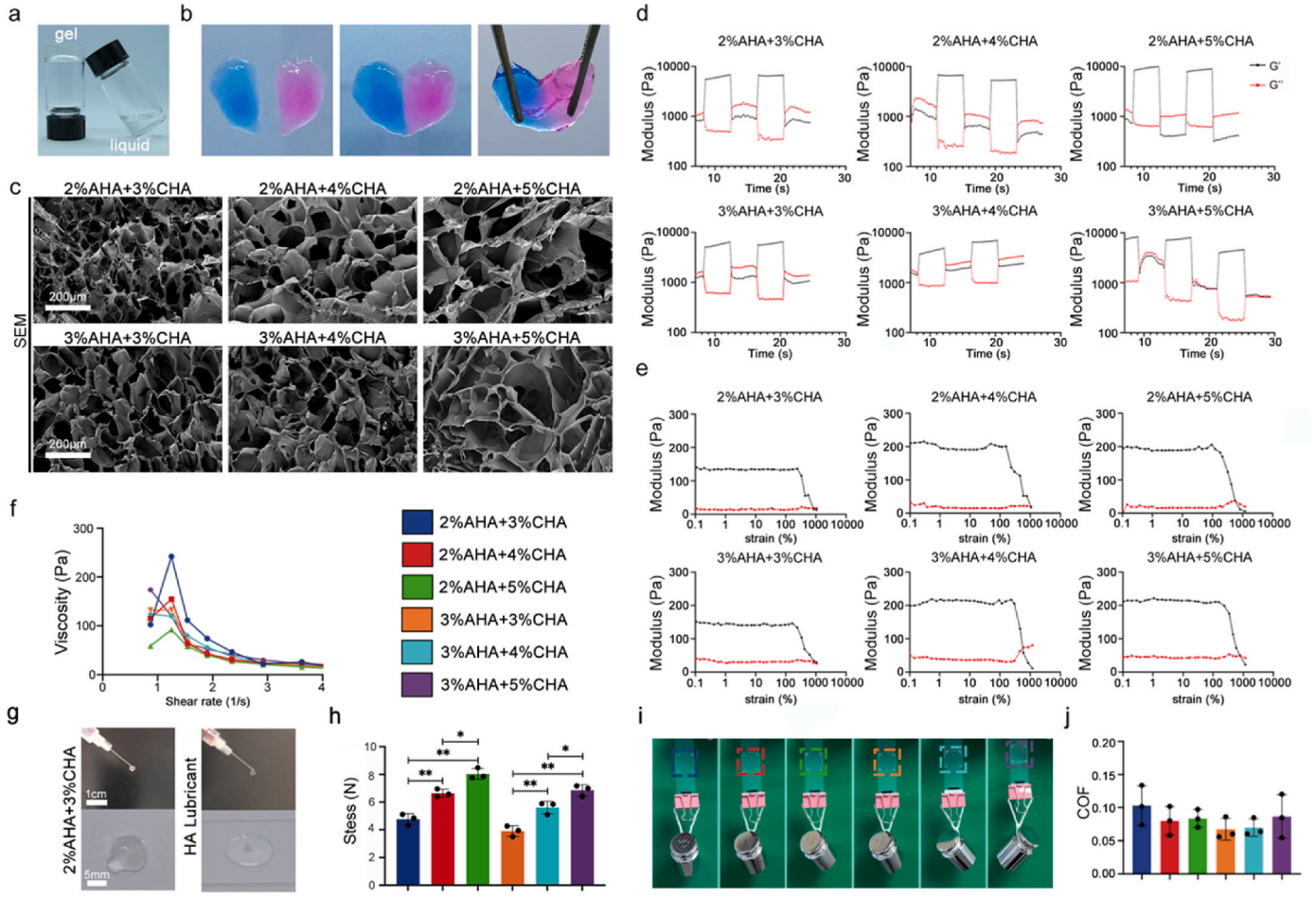

Fig. 3. Material characterization of AHA/CHA hydrogels. a) Photographs of the AHA/CHA hydrogel in its pre- and post-gelation states. b) Photographs of fast self-healing of 2%AHA+3%CHA hydrogel. c) SEM images of AHA/CHA hydrogels. d) G′ and G″ of AHA/CHA hydrogels under alternative step strains of 1 and 350 %. e) G′ and G″ at a constant frequency of 1 Hz and shear strain varying from 0.1 % to 1000 %. f) The viscosity of the AHA/CHA hydrogels. g) Injectability of the AHA/CHA hydrogel and the commercial HA lubricant. h) Adhesion of AHA/CHA hydrogels. i) Each AHA/CHA hydrogel could withstand a weight of 400 g without cracking. j) COF column diagram of AHA/CHA hydrogels. AHA/CHA hydrogels with the same AHA concentration were used for statistical analysis. All data are presented as mean ± SD (n = 3 per group); *p < 0.05; **p < 0.01.

pressure, displaying exceptional adhesion until it eventually succumbs to gravitational forces, resulting in fractures (Videos. S2 and S3). In contrast to the HA lubricant, the AHA/CHA hydrogel demonstrated a longer retention time in vivo, undergoing a gradual degradation and absorption process in approximately 10 days (Fig. S4).

The adhesion ability of AHA/CHA hydrogel was tested by using a universal testing machine. As displayed in Fig. 3h and Table S1, an increase in CHA concentration led to the incorporation of more catechol functional groups within the hydrogel network, subsequently enhancing its adhesion capabilities. Notably, each AHA/CHA hydrogel demonstrated excellent durability, enduring a weight of 400 g against the gravity force without any fragmentation (Fig. 3i). Moreover, macroscopic observation showed that AHA/CHA hydrogel could easily adhere to the surface of mouse knee cartilage (Fig. S5). Intra-articular injection of AHA/CHA hydrogel into the rat knee joints confirmed the ability of the hydrogel to disperse and adhere to the entire articular cartilage surface, potentially contributing to lubrication (Fig. S6).

Furthermore, we measured the coefficients of friction (COFs) of the hydrogels to evaluate their lubricating properties. The COFs were obtained after a 5-min friction test performed on the AHA/CHA hydrogels (Fig. 3j and Fig. S7). The hydrogels in all groups exhibited relatively low COFs, approximately 0.1, with no significant difference among the groups.

After exploring various gelation proportions, we selected two proportions that exhibited superior comprehensive properties, 2 % AHA +3 % CHA and 2 % AHA +5 % CHA. These optimized formulations were then chosen for further investigation in both in vivo and in vitro experiments.

2.2. AHA/CHA hydrogel provides a suitable microenvironment for chondrocytes

To assess the impact of the AHA/CHA hydrogels on chondrocytes, a two-dimensional culture was conducted on the surface of the hydrogels. After culturing for 24 and 48 h, confocal laser microscopy revealed that most chondrocytes remained viable on the AHA/CHA hydrogels (Fig. 4a). Notably, cytoskeleton staining revealed clear F-actin in chondrocytes cultured on the 2 % AHA +3 % CHA hydrogel, indicating that chondrocytes spread better on the 2 % AHA +3 % CHA hydrogel compared to those cultured on the 2 % AHA +5 % CHA hydrogel (Fig. 4b). The proliferation of chondrocytes on AHA/CHA hydrogels was evaluated using the Cell counting Kit-8 (CCK-8) assay (Fig. 4c). The optical density (OD) values demonstrated a consistent increase over time, indicating the sustained viability and proliferative capacity of chondrocytes when cultured on the AHA/CHA hydrogel.

We further investigated the expression of relevant genes in chondrocytes cultured on AHA/CHA hydrogels using quantitative real-time polymerase chain reaction (qRT-PCR) (Fig. 4d). The 2 % AHA +3 % CHA hydrogel group exhibited significantly up-regulated expression of COL2A1, ACAN, and SOX9, compared to the 2 % AHA +5 % CHA hydrogel group. Conversely, the expression of MMP3 and MMP13 was lower in the 2 % AHA +3 % CHA hydrogel group. To corroborate these gene expression trends at the protein level, we conducted western blot (WB) analysis (Fig. 4e). Consistent with the qRT-PCR results, the 2 %

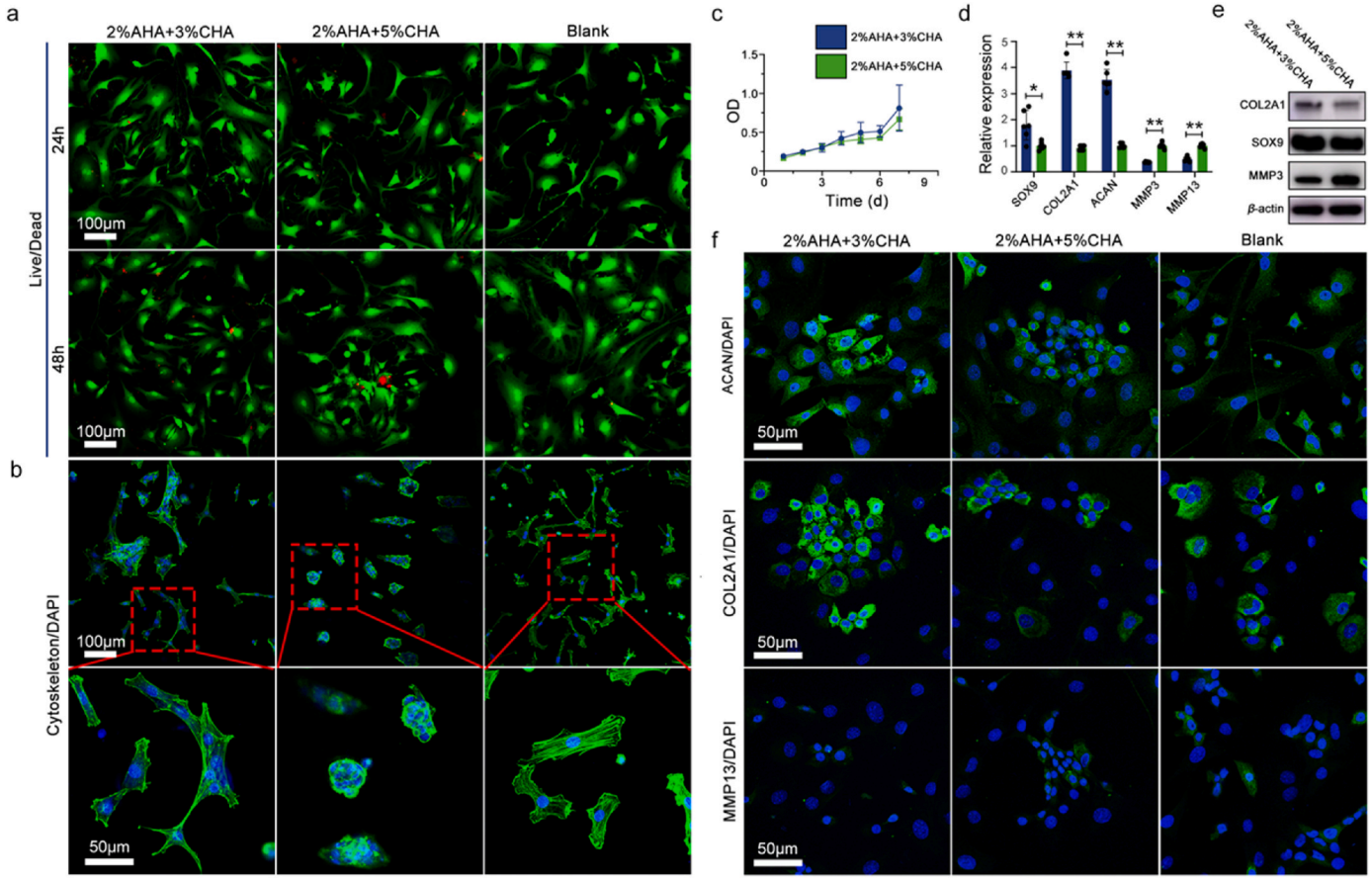

Fig. 4. Cytocompatibility of AHA/CHA hydrogels. a) Live/dead staining of chondrocytes on the AHA/CHA hydrogels. b) Chondrocytes stained by 488-labeled phalloidin. c) The CCK8 assay was performed for 7 days after the chondrocytes were seeded on the AHA/CHA hydrogels. d) Expression of COL2A1, ACAN, SOX9, MMP3 and MMP13 in mouse chondrocytes after 3-day culture on the AHA/CHA hydrogels. e) WB results of ACAN, COL2A1, SOX9 and MMP3 in mouse chondrocytes after 3-day culture on the AHA/CHA hydrogels. f) Immunofluorescence staining of ACAN, COL2A1 and MMP13. All data are presented as mean ± SD (n = 3 per group); *p < 0.05; **p < 0.01.

AHA +3 % CHA hydrogel group displayed obviously higher protein expression of COL2A1 and SOX9, whereas the MMP3 protein expression was conspicuously lower compared to the 2 % AHA +5 % CHA hydrogel group.

According to immunofluorescence staining, chondrocytes cultured on the 2 % AHA +3 % CHA hydrogel expressed more intense immunofluorescence signals for ACAN and COL2A1, which was consistent with the qRT-PCR and WB results (Fig. 4f). Notably, neither the 2 % AHA +3 % CHA nor the 2 % AHA +5 % CHA hydrogels cause an increase in MMP13 immunofluorescence signal intensity in chondrocytes.

2.3. AHA/CHA hydrogels protect articular cartilage in OA

We further validated the therapeutic efficacy of AHA/CHA hydrogels in the early stage of OA in mouse knee joints (at 4 and 6 weeks post-operatively). The extent of subchondral bone sclerosis in the mouse knee joints was assessed using micro-computed tomography (Micro-CT) analysis (Fig. 5a). No significant increase in sclerosis was observed in the subchondral bone plates either in the 2 % AHA +3 % AHA or 2 % AHA +5 % CHA hydrogel groups. The results of the bone mineral density (BMD) analysis conducted on the subchondral bone plates revealed that compared to the PBS group, the two AHA/CHA hydrogel groups showed significantly inhibited BMD increase in the subchondral bone plates (Fig. 5b and Table S2). The cartilage damage was analyzed through Hematoxylin-eosin (HE) and Safranin Orange-fast green staining post-DMM surgery (Fig. 5c and d). In comparison to the PBS group, mice treated with 2 % AHA +3 % CHA hydrogel exhibited reduced cartilage wear and a higher retention of chondrocytes. Mice in the 2 % AHA +5 % CHA hydrogel group showed chondrocyte loss at 4 weeks after DMM surgery, whereas cartilage wear was observed at 6 weeks post-DMM. In the most severe cases, the cartilage disappeared completely. In the PBS group, chondrocytes in the cartilage were completely depleted at 4 weeks post-DMM, and full-thickness cartilage wear was evident at 6 weeks. Conversely, the sham group displayed no cartilage damage.

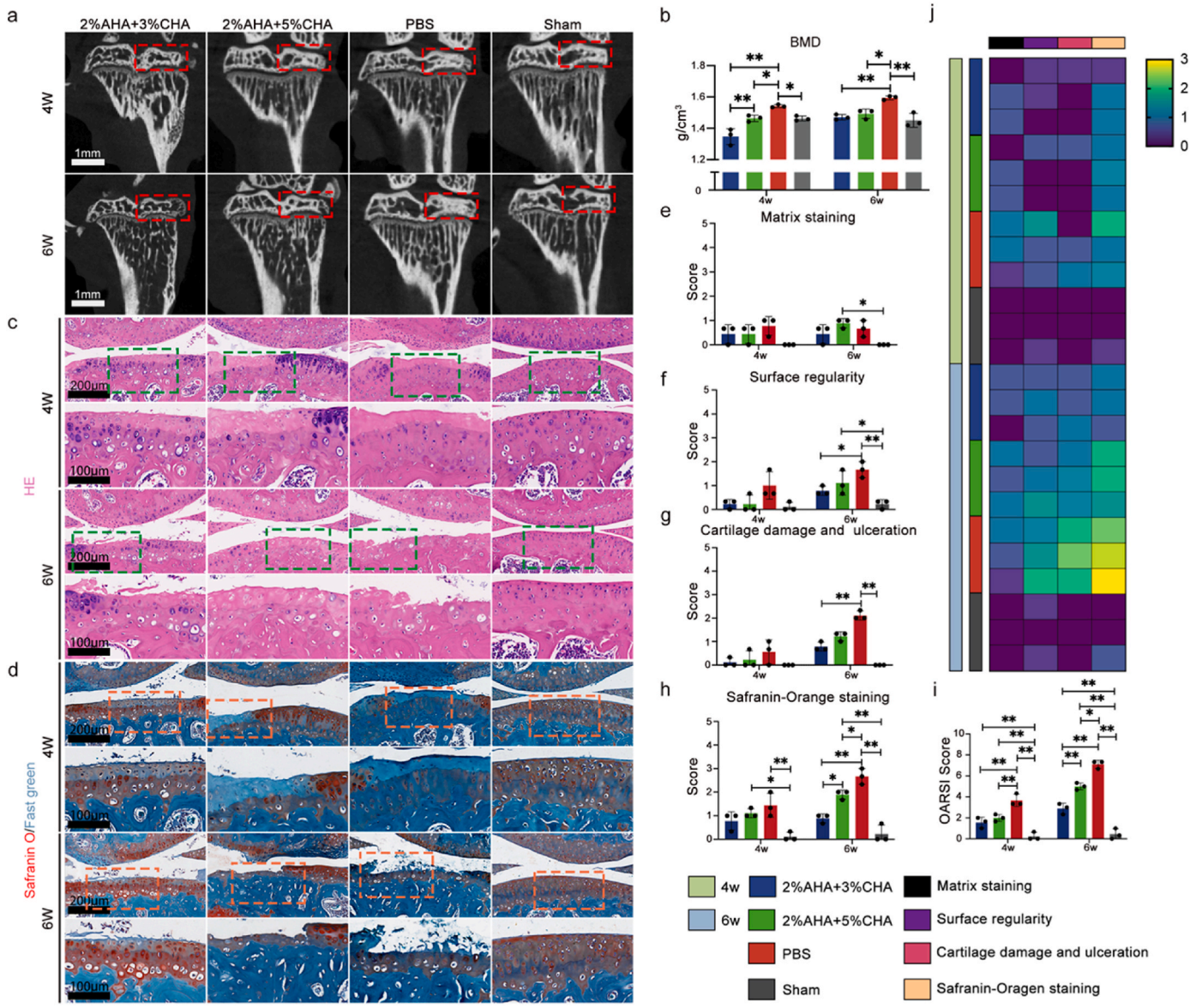

Fig. 5. AHA/CHA hydrogels provide cartilage protection in the knee joint of OA mice. a) Micro-CT analysis images of subchondral bone. b) Quantitative assessment of BMD within the region of interest (ROI) of the subchondral bone plate. c) Hematoxylin-eosin staining. d) Safranin O-fast green staining. e) Matrix staining score. f) Surface regularity score of histological scoring. g) Cartilage damage and ulceration score. h) Safranin Orange staining score. i) OARSI score. j) Heatmap of variables of histological scoring. The scores at the same time point were statistically analyzed. All data are presented as mean ± SD (n = 3 per group); *p < 0.05; **p < 0.01.

Cartilage damage was scored according to the Osteoarthritis Research Society International (OARSI) guidelines, with emphasis on matrix staining, surface regularity, cartilage damage, and safranin staining (Fig. 5e–i) [19]. All scores are listed in Table S3. After visualization of the scores in each group, it was observed that the PBS group exhibited more severe injury, while the 2 % AHA +3 % CHA hydrogel group had the least overall injury (Fig. 5j).

The therapeutic efficacy of AHA/CHA hydrogels in OA mice joints was observed via immunofluorescence staining (Fig. 6 and Table S4). At 4 and 6 weeks after DMM surgery, the cartilage in the 2%AHA+3%CHA group exhibited more ACAN, COL2A1, and SOX9-positive cells and higher immunofluorescence signals compared with that in the 2 % AHA +3 % CHA hydrogel group. The PBS-treated group manifested the characteristic OA phenotype in cartilage, with a marked decrease in ACAN, COL2A1, and SOX9-positive cells. Notably, there was no increase in MMP13-positive cells and fluorescence enhancement in the cartilage of the two hydrogel groups, indicating that the AHA/CHA hydrogels did not cause an inflammatory response in the cartilage.

2.4. AHA/CHA hydrogels mediate signaling pathways related to chondrocyte senescence

To elucidate the underlying mechanism by which AHA/CHA hydrogel protects articular cartilage in OA, RNA sequencing was performed on chondrocytes cultured on the hydrogel to analyze differentially expressed genes (DEGs) in comparison to the Blank group. A total of 866 upregulated and 1235 downregulated DEGs were identified in the 2 % AHA +3 % CHA hydrogel group, as shown in Fig. 7a. A total of 842 upregulated and 1315 downregulated DEGs were identified in the 2 % AHA +5 % CHA hydrogel group. Additionally, 68.75 % of the DEGs overlapped between the 2 % AHA +3 % CHA group and the 2 % AHA +5 % CHA group (Fig. 7b). The heat map analysis revealed a distinct similarity between the DEGs in the two hydrogel groups (Fig. 7c). Gene Ontology (GO) enrichment analysis revealed that among the upregulated DEGs in the 2 % AHA + 3 % CHA hydrogel group, those related to extracellular structure organization, intercellular adhesion regulation, and cartilage development regulation showed significant enrichment, with a high number of genes within these functional

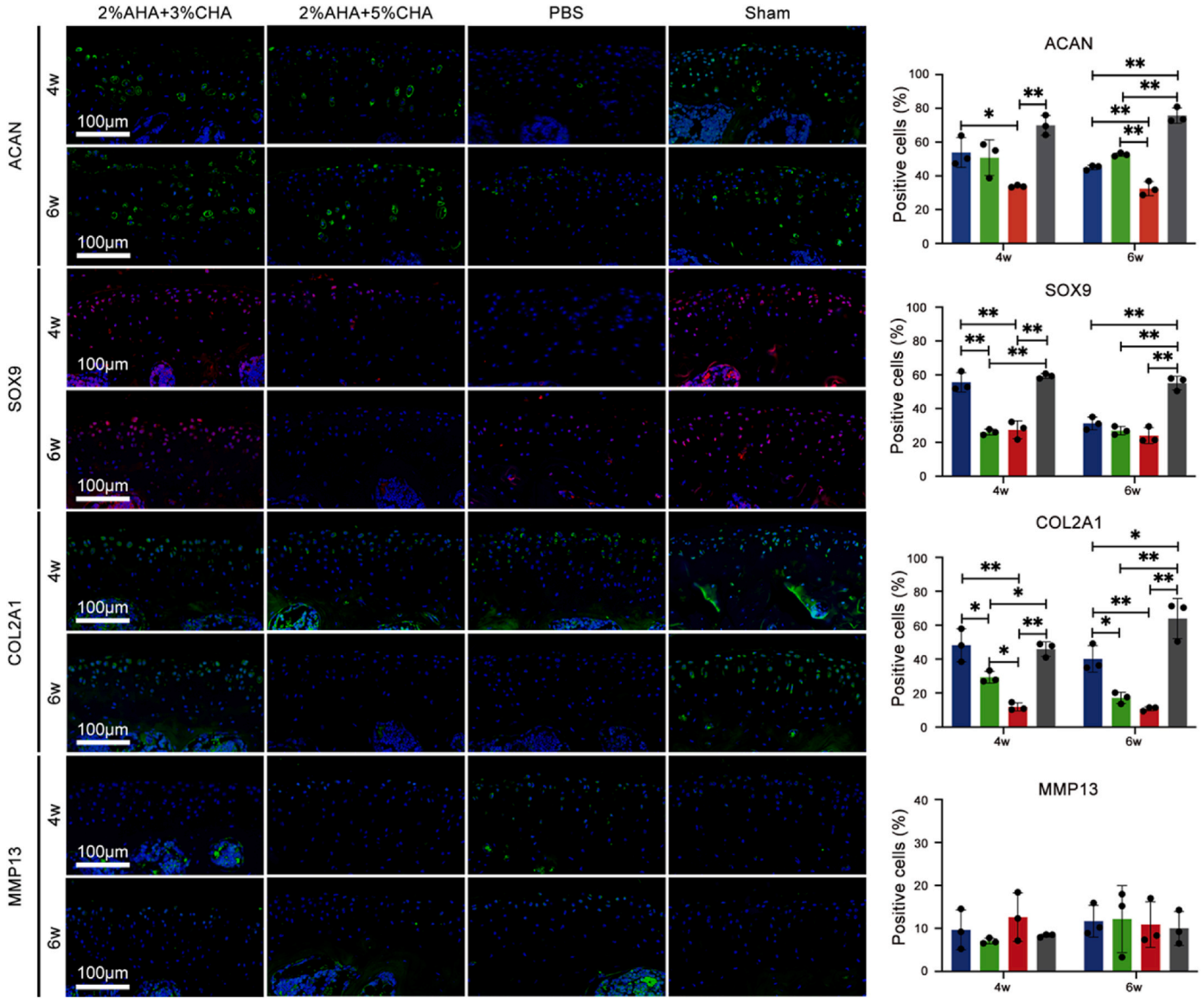

Fig. 6. AHA/CHA hydrogels promote cartilage matrix expression without inflammation. Immunofluorescence staining of ACAN, COL2A1, SOX9, and MMP13 in mouse knee joints at 4 and 6 weeks after DMM surgery. n = 3 per group. Samples at the same time point were statistically analyzed. All data are presented as mean ± SD (n = 3 per group); *p < 0.05; **p < 0.01.

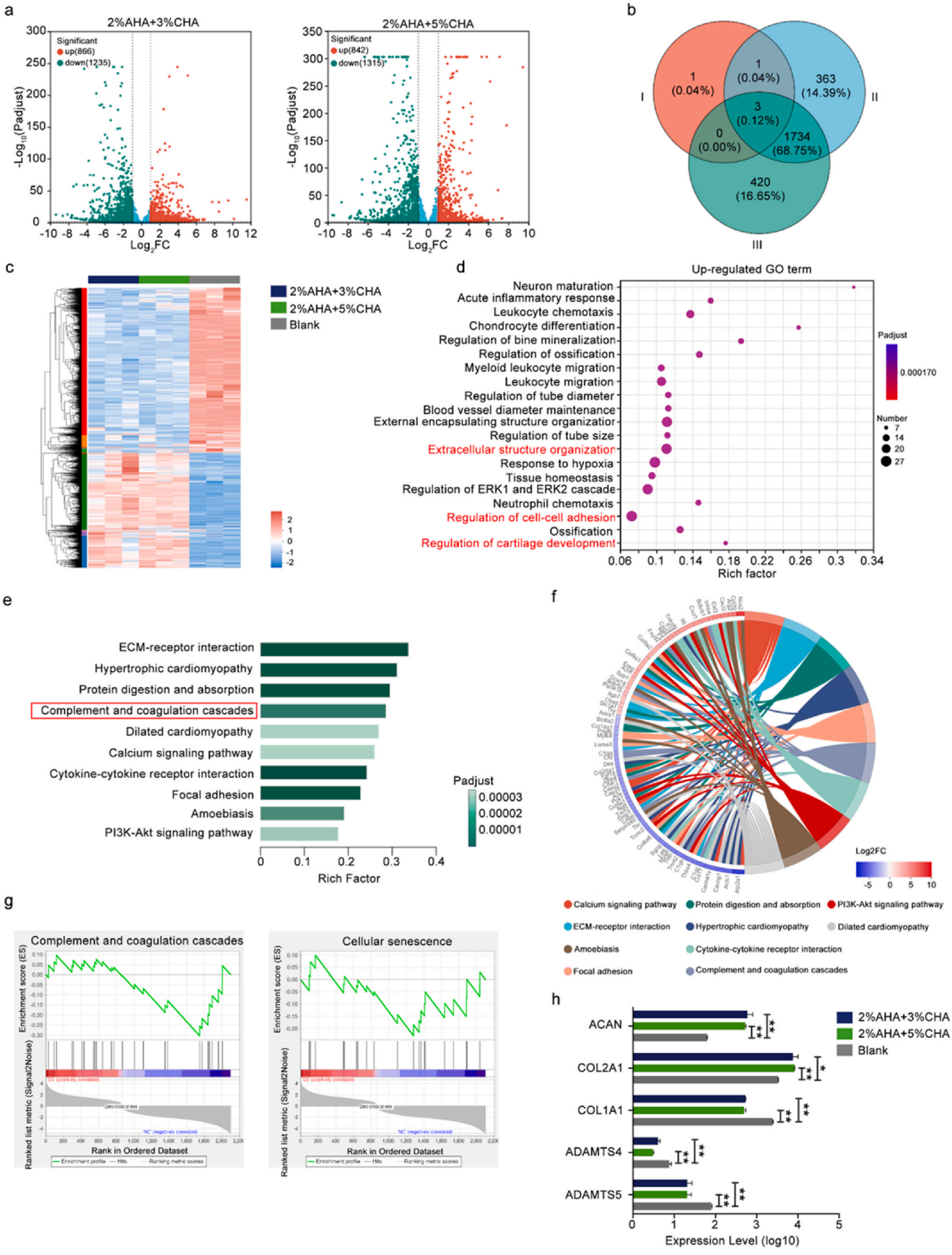

(caption on next page)

Fig. 7. RNA sequencing of chondrocytes cultured on AHA/CHA hydrogel surfaces. a) Volcano plots of differentially expressed genes between AHA/CHA hydrogel group and Blank (fold change >2 or <0.5). b) Venn diagram of differentially expressed genes, I:2%AHA+3%CHA hydrogel group vs 2%AHA+5%CHA hydrogel group, II:2%AHA+3%CHA hydrogel group vs Blank, III:2%AHA+5%CHA hydrogel group vs Blank. c) Heatmap of DEGs between AHA/CHA hydrogel groups and Blank group. d) GO enrichment analysis of upregulated DEGs between 2%AHA+3%CHA hydrogel group and Blank. e) KEGG pathway analysis of DEGs between 2%AHA+3%CHA hydrogel group and Blank group. Pathways are ranked from high to low in terms of enrichment, and heat map is generated according to significance. f) Enriched chord diagrams of KEEG pathway. g) GSEA analysis of complement and coagulation cascades as well as cellular senescence pathways. h) Expression level of OA-related genes in chondrocytes; *p < 0.05; **p < 0.01.

categories being affected (Fig. 7d). GO enrichment analysis and Kyoto Encyclopedia of Genes and Genomes (KEGG) pathway analysis of DEGs in the 2 % AHA + 5 % CHA hydrogel group was also performed (Fig. S8 and Fig. S9). The analysis of DEGs in the group treated with 2 % AHA +5 % CHA hydrogel showed results akin to those observed in the 2 % AHA +3 % CHA group. KEGG pathway analysis of DEGs in the 2 % AHA +3 % CHA group revealed that the four most enriched pathways were ECM-receptor interaction, hypertrophic cardiomyopathy, protein digestion and absorption, as well as coagulation cascade (Fig. 7e and f). Moreover, Gene Set Enrichment Analysis (GSEA) indicated that OA-related pathways, including complement and coagulation cascade as well as cellular senescence, were down-regulated in the 2 % AHA + 3 % CHA group (Fig. 7g). Furthermore, the expression of ACAN and COL2A1 was significantly up-regulated in both AHA/CHA hydrogel groups, while the expression of COL1A1, as well as inflammatory factor genes such as *ADAMTS4* and *ADAMTS5*, was down-regulated (Fig. 7h).

It has been demonstrated that thrombomodulin (THBD) expression is significantly upregulated in aged tissues and chondrocytes [24]. Coagulation cascades primarily manifest through the upregulation of THBD signaling, activating a downstream pathway influencing cell proliferation and migration, known as the THBD pathway. THBD, an anticoagulant receptor, binds to the serine protease thrombin and initiates a proteolytic cascade involving the endothelial protein C receptor (EPCR) and protein C (PC), ultimately leading to G protein-coupled receptor (GPCR) and protease-activated receptor 1 (PAR1) activation [25]. This observation prompted our investigation into gene expression patterns within the THBD pathway (Fig. S10a). It was noted that the expression of the THBD gene in chondrocytes on the AHA/CHA hydrogel surface was significantly inhibited, thereby inhibiting activated protein C (APC) activation. In addition, the gene expression of alpha-2-macroglobulin (A2M) and serine peptidase inhibitor (Serpinb2) was significantly increased, indicating that the activity of serine protease thrombin was significantly inhibited [26]. The expression of serine peptidase inhibitor gene was significantly increased. Moreover, the downregulation of plasminogen activator (Plau) further supported the inhibition of coagulation cascade. In summary, the predictive analysis of the THBD-associated protein network, grounded on RNA sequencing data, offers valuable insights for future verification of this pathway's role in inhibiting OA progression via the AHA/CHA hydrogel (Fig. S10b).

3. Discussion

OA represents a severe and chronic lesion of articular cartilage and bone with approximately 654 million patients worldwide, resulting in a huge medical and economic burden [27]. Aging, obesity, trauma, and infection are common contributing factors. In the early stage of OA, joint cartilage remains structurally intact, despite the presence of pathological factors [28]. However, a decline in HA concentration within synovial fluid, triggered by enzymatic, immunological, and inflammatory processes, severely impacts its viscoelasticity and friction-reducing properties [29]. As OA progresses and lubrication diminishes, cartilage wear, meniscus lesions, synovitis, subchondral bone sclerosis, and osteophyte formation gradually occur in the joint [30]. Consequently, early intervention in OA is crucial to effectively preserve the integrity of cartilage.

The rapid degradation and inherently weak mechanical properties of HA limit the effectiveness of HA synovial fluid supplementation in early OA treatment [31]. To address this challenge, the transformation of HA into a hydrogel has emerged as a promising strategy, leveraging their tunable mechanical properties and extracellular matrix-like structure [32]. HA, abundant in synovial fluid and cartilage tissue, has been explored not only for cartilage defect repair but also for the design of lubricant hydrogels for preventative treatment in the early stages of OA [33,34]. These hydrogels prolong the retention time of HA in vivo and enhance its viscoelasticity, addressing the short metabolic half-life of HA (20 h) in humans [12]. Compared with commercial HA joint lubricants, which suffer from rapid degradation and require frequent intra-articular injections (three to five times weekly), HA hydrogels as synovial fluid lubricants extend the lubrication duration due to their gradual degradation from the hydrogel network to monomeric HA [35]. However, existing HA lubricant hydrogels for early OA stages often exhibit unsuitable modulus, low workability, and adhesion issues, or complex gelation conditions and production processes. To address these limitations, we designed AHA/CHA hydrogel, featuring a straightforward fabrication process, rapid and easy gelation, excellent operability, and suitability for OA treatment. This hydrogel represents an advancement in the field, promising to enhance the efficacy of early OA intervention.

The AHA/CHA hydrogel possesses suitable physical properties for intra-articular application. The results of the self-healing experiments showed that the AHA/CHA hydrogel exhibited rapid self-healing ability, indicating its capability to heal quickly even if it fragmented during joint movements. In addition, previous studies have demonstrated that OA joints exhibit an acidic microenvironment during the process of cartilage degradation [36], and this acidic microenvironment is also essential for the formation of Schiff base cross-linking. Consequently, the cross-linking of AHA/CHA hydrogels remained unaffected in OA joints. The rheometer tests revealed that the AHA/CHA hydrogel could withstand extreme elastic strain, suggesting that the hydrogel effectively adapted to the movement of articular cartilage by deforming when used as a lubricant in joints. However, the 2 % AHA +5 % CHA hydrogel group exhibited a higher cross-linking density, leading to an elevated modulus that might cause a mismatch between the hydrogel modulus and cartilage lubrication. Moreover, the AHA/CHA hydrogel exhibited good injectability and was convenient for intra-articular injection. Therefore, the softer 2 % AHA +3 % CHA hydrogel group is more suitable as a lubricant between articular cartilage.

The AHA/CHA hydrogel has good lubrication ability of articular cartilage. As OA progresses, the impaired lubrication function of synovial fluid leads to an increase in the friction coefficient of articular cartilage up to 0.3 [37,38]. Consequently, the introduction of a wear-reducing, lubricated hydrogel can effectively mitigate OA development. Notably, the AHA/CHA hydrogel maintains a low friction coefficient of approximately 0.1, attributed to the lubricating properties inherent in HA. Under compressive forces between articular cartilage surfaces, the fluid present is almost completely expelled, resulting in partial or full contact of the cartilage surfaces. Therefore, the lubrication mechanism of the cartilage surface introduces the concept of boundary lubrication, in which a thin and adhesive lubricating layer (1–10 nm in thickness) is formed on the contact surface of articular cartilage to prevent full contact under compressive forces [39]. Thus, strengthening the intimate bonding between lubricating hydrogels and cartilage is crucial in designing effective boundary lubrication mechanisms. For example, the covalent connection of lubricating hydrogel to cartilage is an effective stabilizing lubrication method [40]. Additionally, incorporating positively charged liposomes into the hydrogel microspheres presents an intriguing approach, capable of binding to the negatively

charged cartilage via electrostatic interactions, thereby forming a hydrophobic lubricating layer on the cartilage surface [41]. In line with these principles, the AHA/CHA hydrogel is designed to function as a lubricant by strengthening its binding to cartilage through hydrogen bonding, thereby improving the overall lubrication performance. Nevertheless, the strength of hydrogen bonds is modest [42]. The adhesion of AHA/CHA hydrogel does not impede the joint motion, given the controlled volume of hydrogel injected and the limited cartilage adhesion area. Therefore, the AHA/CHA hydrogel emerges as a suitable intra-articular lubricant.

The AHA/CHA hydrogel can provide a suitable extracellular environment for chondrocytes in vitro. In cell experiments, the AHA/CHA hydrogel showed excellent cell compatibility. Chondrocytes showed good adhesion morphology and proliferation ability on the AHA/CHA hydrogel surface. HA can participate in the regulation of cellular activities through various specific binding receptors on the surface of cells, such as cluster determinant 44 (CD44) and receptor for hyaluronan-mediated motility [43]. CD44, as the primary binding receptor of HA on chondrocytes' surface, not only facilitates the biological adhesion between cells and HA but also regulates cell adhesion, migration, and proliferation [44,45]. Chondrocytes utilize the binding of HA to the CD44 receptor to connect the actin cytoskeleton with the local ECM, thereby facilitating the processes of cell migration and adhesion. Moreover, the cell adhesion process involves the activation of the focal adhesion kinase pathway [46]. Interestingly, dopamine modification of HA can enhance cell adhesion. This may be based on the response of the integrin of the chondrocytes with the dopamine group [47–49]. Therefore, the AHA/CHA hydrogel can promote the adhesion and proliferation of chondrocytes due to the osteocyte surface receptor CD44 and dopamine groups. Moreover, the fluorescence intensity of ACAN and COL2A1 was significantly enhanced after chondrocytes were cultured on the surface of 2 % AHA +3 % CHA hydrogel, indicating the synthesis and accumulation of cartilage matrix proteins in chondrocytes. Therefore, the AHA/CHA hydrogel can provide a suitable extracellular environment for chondrocytes.

The AHA/CHA hydrogel improves the extracellular environment of chondrocytes in OA cartilage. In the OA mouse model, the 2 % AHA +3 % CHA hydrogel group showed a better cartilage protection effect. At 6 weeks after DMM, this group exhibited the least cartilage wear, with a significant number of chondrocytes still retained in the cartilage and preservation of the cartilage matrix. In contrast, at 4 weeks post-operation, the PBS group showed complete loss of chondrocytes and destruction of cartilage matrix, indicated by safranin orange staining. Therefore, AHA/CHA hydrogels provide lubrication and improve the extracellular environment within the cartilage matrix, which is crucially important for maintaining the health of endochondral chondrocytes. The AHA/CHA hydrogel network in the joint gradually disintegrated into elongated polymer chains, which subsequently infiltrated the ECM of cartilage and subchondral bone via diffusion, following the endogenous HA metabolic pathway within the joint [50]. The ECM located in the cartilage layer can be improved, thereby promoting the metabolism and synthesis of chondrocytes. In OA, the inflammatory destruction of cartilage leads to the generation of ECM fragments, including HA fragments and fibronectin fragments, which subsequently bind to surface receptors on cartilage and trigger an inflammatory response in chondrocytes [51]. HA could inhibit the activation of p38 mitogen-activated protein kinase (p38 MAPK) phosphorylation by HA fragments and fibronectin fragments by binding to CD44 receptor, thereby inhibiting MMP13 expression [52]. Furthermore, the binding of HA fragment to the CD44 receptor increases the translocation of NF-κB to the nucleus, leading to the upregulation of IL-1β, IL-6, and TNF-α expression, a process that also can be disrupted by the competitive inhibition of HA [53]. In addition, RNA sequencing analysis of chondrocytes cultured on AHA/CHA hydrogels revealed a down-regulation of the THBD pathway, which is significantly associated with chondrocyte senescence. This finding suggests that AHA/CHA hydrogels could potentially offer a pathway to mitigate or arrest chondrocyte senescence.

4. Conclusions

In this study, we developed a novel HA-based hydrogel with excellent self-healing and cartilage surface adhesion capabilities, providing a joint lubricant with low COFs between the articular cartilage surfaces to treat early-stage OA. The AHA/CHA hydrogels demonstrated excellent biocompatibility, creating a favorable microenvironment for chondrocytes. In comparison to the 2 % AHA +5 % CHA hydrogel group, the 2 % AHA +3 % CHA hydrogel group exhibited a suitable low modulus and enhanced efficacy in delaying cartilage surface wear. In RNA sequencing, AHA/CHA hydrogel was found to have a potential pathway that may inhibit chondrocytes senescence. However, the application of AHA/CHA hydrogels in clinical settings requires further validation in larger animals and more rigorous biosafety assessments. Subsequently, we intend to further evaluate the impact of AHA/CHA hydrogels on larger anatomies, such as rabbit and pig knees, under elevated weight-induced stress, with a focus on refining the elastic modulus of the AHA/CHA hydrogels. The signaling pathways identified in this study will also be validated to accumulate additional observational data for potential applications in the treatment of knee-related conditions in humans.

5. Experimental section

5.1. Materials preparation

5.1.1. Materials

If there are no special instructions, all the chemical reagents were purchased from Aladdin.

5.1.2. Synthesis of OHA

1 g of HA (200–400 kDa, Solarbio, China) was dissolved in deionized water. Subsequently, 0.5 g of sodium periodate (Mreda, USA) was added to the solution, which was then allowed to react in a dark environment for 3 h. Following this, 0.5 ml of glycol was introduced into the solution and agitated for a duration of 2 h to effectively neutralize any residual sodium periodate. The solution was then transferred into the dialysis bag (3500 Da) for the purpose of eliminating excess substances through dialysis. After dialysis, the solution was lyophilized and stored at 4 °C for future use.

5.1.3. Synthesis of CHA

1 g of oxidation-modified HA (OHA) was dissolved in deionized water to achieve a concentration of 5 mg/ml. The solution was maintained at a pH of 5.5 throughout the process. 1-(3-Dimethylaminopropyl)-3-ethylcarbodiimide hydrochloride (EDC·HCl) was added to the reaction solution at a molar ratio of 1:1.5 relative to OHA and stirred for 15 min. Subsequently, N-hydroxysuccinimide (NHS) was added at a molar concentration twice that of OHA and stirred for 45 min. Next, dopamine hydrochloride was introduced into the solution in an equal molar amount to OHA, and the solution was stirred at 4 °C for 24 h in an oxygen-free environment. Throughout the stirring period, the solution's pH was maintained within the range of 5.0–6.0. Unreacted chemicals were removed by dialysis with a dialysis membrane (3500 Da) against weakly acidic deionized water. After dialysis, the solution was lyophilized and stored at 4 °C for future use.

5.1.4. Synthesis of AHA

1 g of HA was dissolved in deionized water to achieve a concentration of 10 mg/ml. Adipic acid dihydrazide was added to the solution at a molar ratio of 30 times that of HA and allowed to dissolve fully. The resulting solution was maintained at a pH of 5.0. Next, 9 mmol of EDC·HCl and 1-hydroxybenzotriazole (HOBt) were dissolved in 1 ml of a dimethyl sulfoxide (DMSO, Solarbio, China)/water (1:1) mixture, and

this solution was then added dropwise to the HA solution. The combined solution was stirred for 24 h maintaining a pH of 5.0. The solution was then transferred to a dialysis membrane (8000–14000 Da) and dialyzed against deionized water for 5 days. After dialysis, the solution was lyophilized and stored at 4 °C for future use.

5.2. Materials characterization

5.2.1. FTIR analysis

The samples were analyzed using a Fourier Transform Infrared spectrometer (Thermo Fisher, USA). In the Attenuated Total Reflectance (ATR) mode, all spectra are scanned 32 times in the wavenumber region of 4000–500 cm^{-1}.

5.2.2. ^1H NMR spectroscopy analysis

The samples were dissolved in deuterated water, and the hydrogen atoms were analyzed by ^1H NMR at 600 MHz with a base frequency resolution of 0.1 Hz (Agilent, USA). The acyl hydrazide substitution degree (DS) of AHA was determined by calculating the accumulated area ratio between the characteristic peak of adipic hydrazide (δ 1.3–1.5 ppm) in the spectrum and the characteristic proton peak on the carbon ring of hyaluronic acid (δ 3.0–4.0 ppm), using the following formula [20]:

$$DS = \frac{\delta(1.3 \sim 1.5)/4}{\delta(3.0 \sim 4.0)/10} \times 100\% = \frac{2.72/4}{10.77/10} = 63.1\%$$

The dopamine substitution degree of CHA was determined by calculating the ratio of the accumulated area of the characteristic catechol peak (δ 2.8 ppm) to the N-$COCH_3$ peak at the end of the carbon ring (δ 1.9 ppm) in the spectrum. The formula used for this calculation is as follows [54]:

$$DS = \frac{\delta 2.8/2}{\delta 1.9/3} \times 100\% = \frac{2.75/2}{9.22/3} = 44.7\%$$

5.2.3. Oxidation level of OHA

The degree of aldehyde group modification, was determined by quantifying the volume of NaOH solution consumed using the hydroxylamine hydrochloride method [40]. 0.1 g of OHA was dissolved in 25 ml of hydroxylamine hydrochloride solution containing 0.0003 wt% methyl orange reagent (prepared by solution dilution) (0.25 mol/L, pH = 4.5) and stirred for 24 h. Then, the aldehydes were converted to oxime, and hydrochloric acid was released by titration with 0.1 mol/L NaOH solution, during which the pH value was recorded with a pH meter. The volume of NaOH solution consumed (ΔV) in the burette was recorded until the pH reached 5.0. The titration was stopped when the colour of the solution changed from red to yellow.

Experiments were repeatedly performed three times to calculate the average degree of oxidation, which was using the following formula:

$$Oxidation\% = \frac{403c \times \Delta V \times 10^{-3}}{2w} \times 100\% = \frac{403 \times 0.1 \times 2.9 \times 10^{-3}}{2 \times 0.1} = 58.4\%$$

c in the formula represents the molar concentration of sodium hydroxide solution. w represents the weight of the HA sample.

5.2.4. Gelation assays

Solutions of 2 % and 3 % AHA were prepared by adding 1 ml of deionized water to 20 mg and 30 mg of AHA, respectively. The 4 % AHA did not completely dissolve to form a homogeneous solution, and therefore it was not considered. Solutions of 3 %, 4 % and 5 % CHA were prepared in the same way. All AHA and CHA solutions in this paper were mixed in a 2:1 vol ratio. The time required to complete the gelation process was recorded. To assess the stability of the hydrogels, the glass bottles containing them were inverted for 10 min to observe whether they flowed under the influence of gravity [19].

5.2.5. Self-healing assays

Macroscopic self-healing tests were conducted to observe the self-healing capacity of AHA/CHA hydrogels [55]. Rhodamine B and methylene blue were used to stain two pieces of AHA/CHA hydrogel, respectively. Then, the two stained pieces were placed next to each other on a glass slide. The time required for complete self-healing was recorded. Then, the healed hydrogel was grabbed with forceps and pulled apart to observe whether it healed as a single unit. In a separate experiment, a piece of AHA/CHA hydrogel was cut open, and the healing process of the cut interface was photographed under an optical microscope while the time required for healing was recorded.

5.2.6. Micromorphology

The Micromorphology of the AHA/CHA hydrogel was photographed using the Nova Nano 450 Scanning Electron Microscopy (SEM, Thermo FEI, Czech Republic). A 2-mm thick slice of lyophilized hydrogel was placed on the platform surface and sprayed with platinum. Then, the samples were observed on the instrument. The ImageJ software was utilized for measuring porosity and pore diameter.

5.2.7. Adhesion tests

The adhesion strength of the AHA/CHA hydrogels was tested using a universal material testing machine (Roell Z020, Zwick, Germany). The AHA and CHA solutions were applied separately to the rectangular area of 25 mm × 25 mm on the slides. After the glass sheets coated with AHA and CHA solutions were fitted together, they were left to undergo the gelation process. Two adherent slides were then loaded with 400 g weights in the direction of gravity to assess whether the hydrogel would fragment. To determine the maximum tensile stress (hydrogel breakage) between the two slides after hydrogel adhesion, the universal testing machine, equipped with a 500 N sensor, was used, with the tensile rate set at 1 mm/min.

5.2.8. Rheological measurements

The rheological properties of the hydrogels were measured using a Rotating Rheometer (MARS 60, HAAKE, Germany) at 25 °C. A 20-mm parallel plate was selected. The AHA and CHA solutions were uniformly mixed on the plate to prepare the AHA/CHA hydrogel of fixed volume. The test was conducted according to the following settings:

The hydrogel was subjected to a constant oscillation frequency of 1 Hz. Each sample was tested for 210 s, with 40 data points recorded.

The oscillation frequency was set to a constant value of 1 Hz, the shear strain γ was varied from 0.1 % to 1000 % according to a logarithmic scale. The time interval between data points was set to 3 s per point to observe the changing trend of the loss modulus G'' and the storage modulus G' within this shear strain range.

To assess the self-healing ability of the AHA/CHA hydrogels, strain scans were performed at a constant frequency (10 rad/s) with a minor strain of 1 % and an enormous strain of 350 %, repeated in three cycles of 240 s each.

To evaluate the shear viscosity of the hydrogel through flow scanning experiments, a linear gradient shear rate ranging from 1 to 40 1/s was applied, and the viscosity was measured at different shear rates.

5.2.9. Friction test

The friction coefficient of the AHA/CHA hydrogel was measured using a Friction Testing Machine (Bruker, USA). The friction test was conducted on the surface of the hydrogel using a GCr15 steel ball with a diameter of 5 mm. A linear reciprocating motion was applied to the steel ball at a frequency of 1 Hz for 5 min under a load of 1 N. Three replicate samples from each group were used for the experiment.

5.2.10. Sterilization of AHA and CHA solutions

AHA and CHA were exposed to ultraviolet light for a duration of 2 h, subsequently dissolved in sterile deionized water, and finally filtered through a 0.22 μm membrane filter unit. All operations were completed

on a sterile workbench.

5.3. In vitro experiments

5.3.1. Isolation of mouse primary chondrocytes

Primary chondrocytes were isolated from the femoral condyle of 1-day-old C57/BL mice. The mice were euthanized and subsequently immersed in 75 % ethanol for a duration of 10 min. Knee cartilage from the mice was removed under sterile conditions using microscopic instruments and washed three times with PBS. The chopped cartilage was added to DMEM medium (Gibco, USA) containing collagenase type II (2.5 mg/ml) and digested overnight in a cell incubator. Chondrocytes were collected by filtration using a cell filter with a pore size of 75 μm, followed by centrifugation at 1000 rpm for 5 min. The chondrocytes were cultured in a complete DMEM medium, which contained 5 % fetal bovine serum (FBS, CellMax, China) and 1 % penicillin-streptomycin (Thermo Fisher Scientific, USA). The chondrocytes were designated as P0, and the generation number was incremented by 1 after each digestion. The P2 generation was used by default for chondrocytes in all subsequent cell experiments.

5.3.2. Cytocompatibility assays

Chondrocytes were cultured in two-dimensions on AHA/CHA hydrogels surface. The biocompatibility of the AHA/CHA hydrogel was evaluated using Cell Count Kits 8 (CCK8, APExBio, USA) and Calcein/PI Cell Viability/Cytotoxicity Assay Kit (Beyotime, China). Sterile AHA and CHA solutions were mixed at the bottom of a 24-well plate. The groups included: 2 % AHA +3 % CHA group, 2 % AHA +5 % CHA group and Blank group (no hydrogel was added). After cross-linking of the hydrogel was completed, 500 μl of complete DMEM mediums was added. Mouse chondrocytes were seeded on the AHA/CHA hydrogel surface at a density of 2×10^5 cells/well. Chondrocytes with the AHA/CHA hydrogel were cultured for 24 and 48 h. According to the manual, the cell live/dead staining solution was added and allowed to react for 30 min. The fluorescence image of chondrocytes was photographed by a Nikon A1 Ti confocal microscope (Nikon, Japan).

Sterile AHA and CHA solutions were mixed at the bottom of a 96-well plate. The groups included: 2 % AHA +3 % CHA group and 2 % AHA +5 % CHA group. After the completion of cross-linking, 100 μl of complete DMEM medium was added. Mouse chondrocytes were seeded on the AHA/CHA hydrogel surface at a density of 2×10^4 cells/well and cultured for 1, 3, 5 and 7 days. The cells were treated with 100 μl of complete DMEM medium supplemented with 10 % (v/v) CCK-8 and incubated at 37 °C for 2 h. Absorbance at a wavelength of 450 nm was measured using a microplate photometer (Thermo, USA).

5.3.3. Cytoskeleton staining

The cytoskeleton of mouse chondrocytes on the AHA/CHA hydrogel was observed by staining F-actin with CoraLite® Plus 488-Phalloidin (Proteintech, China). Sterile AHA and CHA solutions were mixed at the bottom of a 24-well plate. The groups included: 2 % AHA +3 % CHA group, 2 % AHA +5 % CHA group, and Blank group. After gelation of the hydrogel was completed, 500 μl of complete DMEM mediums was added. Mouse chondrocytes were seeded on the AHA/CHA hydrogel surface at a density of 2×10^5 cells/well and cultured for 3 days.

After washing with PBS, the chondrocytes were fixed in 4 % paraformaldehyde for 15 min. The samples were washed three times with PBS, followed by incubation in 0.3 % Triton X-100 (Sigma-Aldrich, USA) solution for a duration of 5 min. Lastly, chondrocytes were stained with 4',6-diamidino-2-phenylindole (DAPI, Solarbio, China) and CoraLite® Plus 488-Phalloidin, and observed using a Nikon A1 Ti confocal microscope (Nikon, Japan).

5.3.4. Western blot

Sterile AHA and CHA solutions were mixed at the bottom of a 6-well plate. The groups included: 2 % AHA +3 % CHA group and 2 % AHA +5 % CHA group. After complete cross-linking of the hydrogel, 2 ml of complete DMEM medium was added. Mouse chondrocytes were seeded on the surface of the hydrogels at a density of 2×10^6 cells/well and cultured for 3 days.

Cells were lysed using pKill solution (0.05 % Tris-HCl, pH 6.8, 0.01 g/ml sodium dodecyl sulfate, SDS) containing 100 mM phenylmethanesulfonyl fluoride (PMSF, Fdbio, China). The protein concentration of each sample was adjusted to an equal level. Proteins were separated on 10 % SDS-PAGE gels (Genefirst, USA) and transferred onto polyvinylidene fluoride membranes (Bio-Rad, USA). The membranes were incubated in 5 % nonfat milk for 1 h on a shaker at room temperature, followed by incubation with the primary antibody at 4 °C on a shaking platform overnight. Subsequently, the membranes were washed three times with Tris-Buffered Saline (TBS, HaoKebio, China) containing 0.1 % Tween-20 (Fdbio, China). The secondary antibody solution, prepared in accordance with the manufacturer's instructions utilizing 5 % nonfat milk, was added to the membranes, which were then shaken for 1 h. Protein bands were visualized using Fdbio-Pico Ecl (Fdbio, China) and a chemiluminescence system (ChemiDocTM Touch Imaging System, Bio-Rad, USA).

The antibodies used in this study are listed in Table S5.

5.3.5. qRT-PCR

The total RNA was isolated and purified from mouse chondrocytes using the AG RNAex Pro Reagent (AG Accurate Biology, China) and the Steady-Pure RNA Extraction Kit (AG Accurate Biology, China). The mRNA was reverse transcribed into cDNA using Evo M-MLVRT Premix (AG Accurate Biology, China). qRT-PCR was conducted using Hieff® qPCR SYBR Green Master Mix (Yeasen, China) on a 96 real-time PCR detection system (QuantStudio 6 Flex, Thermo, USA). The relative expression levels of the target genes were quantitatively evaluated employing the $2^{-\Delta\Delta Ct}$ method, a standardized approach for gene expression analysis. The primer sequences utilized in this study are comprehensively outlined in Table S6.

5.3.6. Cellular immunofluorescence

Sterile AHA and CHA solutions were mixed at the bottom of a 24-well plate. The groups included: 2 % AHA +3 % CHA group, 2 % AHA +5 % CHA group and Blank group. After complete cross-linking of the hydrogel, 2 ml of complete DMEM medium was added to each well. Mouse chondrocytes were seeded on the surface of the AHA/CHA hydrogel at a density of 2×10^5 cells/well and cultured for 3 days. After removing the medium, the cells were washed in PBS three times and then fixed in 4 % paraformaldehyde for 10 min. Following three additional washes in PBS, the cells were treated with 0.3 % Triton X-100 solution for 5 min, followed by incubation with 1 % FBS solution for 1 h. Anti-MM13, anti-ACAN, anti-COL2A1 and anti-SOX9 were diluted with the primary antibody diluent according to the recommended ratios in the instructions. The cells were subsequently incubated with the primary antibodies overnight at 4 °C. After removing the primary antibodies and washing the wells in PBS three times, the chondrocytes were incubated with goat anti-mouse or goat anti-rabbit secondary antibody for 1 h, followed by washes in PBS three times. Subsequently, chondrocytes were incubated in the prepared DAPI solution for 15 min, which was diluted using PBS at a ratio of 1:200. The chondrocytes were photographed using a Nikon A1 Ti confocal microscope (Nikon, Japan). The number of positive cells was calculated using ImageJ.

5.3.7. RNA sequencing

Mouse chondrocytes were seeded on sterile AHA/CHA hydrogels at 2×10^6 cells/well for 3 days ($n = 3$). The cells underwent total RNA extraction utilizing the TRIzol® Reagent, strictly adhering to the manufacturer's guidelines. Subsequently, the RNA purification process, reverse transcription, library construction, and sequencing were carried out by Shanghai Majorbio Bio-pharm Biotechnology Co., Ltd. (Shanghai, China), with each step meticulously following the prescribed protocols

provided by the respective manufacturers.

5.4. In vivo experiment

5.4.1. Animals

All animal experiments were approved by the Animal Ethics Committee of Zhejiang University (ethical approval number: ZJU20240659). A total of 28 male C57/BL (6 weeks old, weighing 25 ± 2 g) and 28 male Sprague-Dawley (SD) rats (6 weeks old, weighing 150 ± 3 g) were sacrificed in this study. Each animal was anesthetized with pentobarbital (40 mg kg^{-1}) and operated under sterile conditions.

5.4.2. Degradability of AHA/CHA hydrogel in vivo

The 2 % AHA +3 % CHA hydrogel was chosen to assess the degradability. The commercial HA lubricant (ARTZ Dispo) was purchased from Seikagaku Corporation. Twenty-eight 6-week-old SD male rats were divided into two groups: the hydrogel group and the HA lubricant group. After anesthesia, rats were injected with 500 μl of the AHA/CHA hydrogel or HA lubricant into the subcutaneous layer. The rats were euthanized at 3-day intervals and subsequently underwent skin sample collection.

5.4.3. Distribution of the AHA/CHA hydrogel in joint

Fluorescent labeling of AHA was prepared by conjugating an NHS derivative of a fluorescent dye to the primary amine group on AHA [56]. First, the reaction between Cy7-SE (Goyoobio, China) and AHA solution was conducted overnight at room temperature in the dark, followed by the removal of unbound Cy7-SE through dialysis. After administering anesthesia to 6-week-old SD rats, a total volume of 40 μl of the 2 % AHA +3 % CHA hydrogel was injected into the knee joint of each rat. After 24 h, the knee joints were reopened and observed.

5.4.4. Mouse OA model

The DMM surgery was conducted according to a previously reported procedure with slight modification [57]. The medial meniscal tibial ligaments of both knees of 21 mice were cut with scissors and sutured. The mice undergoing DMM surgery were randomly allocated into three groups (2 % AHA + 3 % CHA, 2 % AHA + 5 % CHA, or PBS) after 1 week and treated as follows:

2 % AHA + 3 % CHA group: sterile 2 % AHA and 3 % CHA solutions were mixed until they formed a gel. Then, 10 μl of the hydrogel was injected intra-articularly using an insulin needle.

2 % AHA +5 % CHA group: sterile 2 % AHA and 5 % CHA solutions were mixed until they formed a gel. Then, 10 μl of the hydrogel was injected intra-articularly using an insulin needle.

PBS group: 10 μl of PBS was injected intra-articularly using an insulin needle.

In the Sham group, 7 mice underwent bilateral knee joint incision, followed by direct suture, after being washed with physiological saline. After 1 week, 10 μl of PBS was injected intra-articularly using an insulin needle.

Knee joint samples were collected at 4 and 6 weeks post-DMM, following euthanasia of the mice.

5.4.5. Micro-CT

The microstructure of the subchondral bone in the mouse knee joint was analyzed using SkyScan1173 Micro-Computed Tomography (micro-CT, SkyScan, Belgium). Micro-CT 3D Visualization Software (Micro Photonics Inc, USA) was used to reconstruct the images of knee joints, and the subchondral bone of the tibia condyle was selected as the region of interest (ROI). The ROI contours were delineated in CT-Analysis software (SkyScan, Belgium), and the BMD values of 100 slices were uniformly analyzed.

5.4.6. Histological analysis

Mouse knee joints were immersed in 4 % paraformaldehyde solution for 1 day and then in EDTA decalcified solution (Macklin, China) for 10 days. EDTA Decalcified Solution was refreshed once a day. Excess tissue surrounding the knee joints was trimmed while ensuring the integrity of the joint capsule. After paraffin embedding, the knee joint was sliced to sections of 7 μm thickness. The paraffin sections were sequentially immersed in xylene, followed by a gradient alcohol series, and finally submerged in deionized water. Subsequently, HE staining and Safranin O-fast green staining (1 % Safranin O, 0.5 % fast green; Sigma, USA) were conducted to assess the articular cartilage damage. The slides were scanned using an automatic digital slice scanning system (Kfbio, China) at uniform magnification.

5.4.7. Immunofluorescence

Paraffin sections were sequentially immersed in xylene, followed by a gradient alcohol series, and finally submerged in deionized water. According to the instructions, the sodium citrate antigen retrieval solution (Solarbio, China) was diluted to the working concentration with deionized water. Sections were immersed in antigen retrieval solution at 55 °C overnight. After that, sections were soaked in PBS for 5 min and this step was repeated three times, followed by immersion in 0.3 % TritonX-100 solution for 5 min. Sections were then immersed in 1 % FBS solution for 2 h. Anti-MMP13, anti-ACAN, anti-COL2A1 and anti-SOX9 antibodies (Table S5) were diluted with the primary antibody diluent according to the recommended ratio in the manufacturer's instructions. Next, sections were incubated with the primary antibody solution overnight at 4 °C. Afterwards, the sections were subjected to three consecutive immersions in PBS, each lasting 5 min, followed by a 1-h incubation period with the appropriate secondary antibody solution. Finally, sections were incubated with DAPI solution for 15 min. Sections were scanned using Olympus VS120 Virtual Slide Scanning System (Olympus, Japan).

5.4.8. Osteoarthritis score

Cartilage degeneration was assessed using the OARSI scoring system by three blinded observers. The scoring results of the section were analyzed after averaging.

5.5. Statistical analysis

Statistical analysis was conducted using SPSS software. The significant differences among the groups in Fig. 3h and j, Fig. S2, Fig. S7, Fig. 5b–e, f, g, h and i were analyzed using one-way ANOVA. The significant difference between groups in Fig. 4d was analyzed using T test. To discern DEGs between two distinct groups in Fig. 7, we quantified the expression level of each transcript employing the transcripts per million reads (TPM) normalization approach. Subsequently, we conducted differential expression analysis utilizing the DESeq2 package, a widely adopted tool for identifying statistically significant changes in gene expression between conditions. $|\log2FC| >= 1$ and padjust <0.05 were considered to be significantly DEGs. Data are represented as mean ± standard deviation. Statistical significance in all graphs is indicated by * ($p < 0.05$), ** ($p < 0.01$).

CRediT authorship contribution statement

Dongze Wu: Writing – original draft, Resources, Methodology, Investigation. **Shuhui Yang:** Methodology, Investigation, Formal analysis. **Zhe Gong:** Investigation, Formal analysis. **Xinxin Zhu:** Investigation. **Juncong Hong:** Software, Investigation. **Haitao Wang:** Software, Methodology. **Wenbin Xu:** Investigation, Formal analysis. **Juncheng Lai:** Writing – review & editing. **Xiumei Wang:** Project administration. **Jiye Lu:** Project administration, Conceptualization. **Xiangqian Fang:** Validation, Supervision. **Guoqiang Jiang:** Validation, Supervision, Resources. **Jinjin Zhu:** Validation, Supervision, Project administration, Conceptualization.

Declaration of competing interest

The authors declare that they have no known competing financial interests or personal relationships that could have appeared to influence the work reported in this paper.

Acknowledgments

This work was supported by grants from the National Natural Science Foundation of China (82302712, 32301144, 82101647), China Post-doctoral Science Foundation (2023M743056), the Natural Science Fund of Zhejiang Province (Q24H060012, Q24C100012, Y23H060039), and the Medical Science and Technology Project of Zhejiang Province (2023RC027, 2024KY1107), Union Fund Project of National Natural Science Foundation of China (U22A20282).

Appendix A. Supplementary data

Supplementary data to this article can be found online at https://doi.org/10.1016/j.mtbio.2024.101353.

Data availability

Data will be made available on request.

References

[1] H. Kotlarz, C.L. Gunnarsson, H. Fang, J.A. Rizzo, Insurer and out-of-pocket costs of osteoarthritis in the US: evidence from national survey data, Arthritis Rheum. 60 (2009) 3546–3553, https://doi.org/10.1002/art.24984.
[2] J. Martel-Pelletier, A.J. Barr, F.M. Cicuttini, P.G. Conaghan, C. Cooper, M. B. Goldring, S.R. Goldring, G. Jones, A.J. Teichtahl, J.-P. Pelletier, Osteoarthritis, Nat. Rev. Dis. Prim. 2 (2016) 16072, https://doi.org/10.1038/nrdp.2016.72.
[3] R.C. Gupta, R. Lall, A. Srivastava, A. Sinha, Hyaluronic acid: molecular mechanisms and therapeutic trajectory, Front. Vet. Sci. 6 (2019), https://doi.org/10.3389/fvets.2019.00192.
[4] S. Glyn-Jones, A.J.R. Palmer, R. Agricola, A.J. Price, T.L. Vincent, H. Weinans, A. J. Carr, Osteoarthritis, Lancet 386 (2015) 376–387, https://doi.org/10.1016/S0140-6736(14)60802-3.
[5] B. Abramoff, F.E. Caldera, Osteoarthritis, Medical Clinics of North America, vol. 104, 2020, pp. 293–311, https://doi.org/10.1016/j.mcna.2019.10.007.
[6] G.-I. Im, The concept of early osteoarthritis and its significance in regenerative medicine, Tissue Eng Regen Med 19 (2022) 431–436, https://doi.org/10.1007/s13770-022-00436-6.
[7] J.N. Katz, K.R. Arant, R.F. Loeser, Diagnosis and treatment of hip and knee osteoarthritis, JAMA 325 (2021) 568, https://doi.org/10.1001/jama.2020.22171.
[8] C. Li, Z. Cao, W. Li, R. Liu, Y. Chen, Y. Song, G. Liu, Z. Song, Z. Liu, C. Lu, Y. Liu, A review on the wide range applications of hyaluronic acid as a promising rejuvenating biomacromolecule in the treatments of bone related diseases, Int. J. Biol. Macromol. 165 (2020) 1264–1275, https://doi.org/10.1016/j.ijbiomac.2020.09.255.
[9] L. Martin-Alarcon, A. Govedarica, R.H. Ewoldt, S.L. Bryant, G.D. Jay, T.A. Schmidt, M. Trifkovic, Scale-dependent rheology of synovial fluid lubricating macromolecules, Small 20 (2024), https://doi.org/10.1002/smll.202306207.
[10] C.N. Bertolami, T. Gay, G.T. Clark, J. Rendell, V. Shetty, C. Liu, D.A. Swann, Use of sodium hyaluronate in treating temporomandibular joint disorders: a randomized, double-blind, placebo-controlled clinical trial, J. Oral Maxillofac. Surg. 51 (1993) 232–242, https://doi.org/10.1016/S0278-2391(10)80163-6.
[11] C. Cooper, F. Rannou, P. Richette, O. Bruyère, N. Al-Daghri, R.D. Altman, M. L. Brandi, S. Collaud Basset, G. Herrero-Beaumont, A. Migliore, K. Pavelka, D. Uebelhart, J. Reginster, Use of intraarticular hyaluronic acid in the management of knee osteoarthritis in clinical practice, Arthritis Care Res. 69 (2017) 1287–1296, https://doi.org/10.1002/acr.23204.
[12] D.J. Hunter, Viscosupplementation for osteoarthritis of the knee, N. Engl. J. Med. 372 (2015) 1040–1047, https://doi.org/10.1056/NEJMct1215534.
[13] A. Gilpin, Y. Zeng, J. Hoque, J.H. Ryu, Y. Yang, S. Zauscher, W. Eward, S. Varghese, Self-healing of hyaluronic acid to improve in vivo retention and function, Adv. Healthcare Mater. 10 (2021), https://doi.org/10.1002/adhm.202100777.
[14] Z. Cai, H. Zhang, Y. Wei, M. Wu, A. Fu, Shear-thinning hyaluronan-based fluid hydrogels to modulate viscoelastic properties of osteoarthritis synovial fluids, Biomater. Sci. 7 (2019) 3143–3157, https://doi.org/10.1039/C9BM00298G.
[15] M. Teodorescu, M. Bercea, S. Morariu, Biomaterials of PVA and PVP in medical and pharmaceutical applications: perspectives and challenges, Biotechnol. Adv. 37 (2019) 109–131, https://doi.org/10.1016/j.biotechadv.2018.11.008.
[16] M. Chen, P. Yu, J. Xing, Y. Wang, K. Ren, G. Zhou, J. Luo, J. Xie, J. Li, Gellan gum modified hyaluronic acid hydrogels as viscosupplements with lubrication maintenance and enzymatic resistance, J. Mater. Chem. B 10 (2022) 4479–4490, https://doi.org/10.1039/D2TB00421F.
[17] J. Chen, J. Yang, L. Wang, X. Zhang, B.C. Heng, D.-A. Wang, Z. Ge, Modified hyaluronic acid hydrogels with chemical groups that facilitate adhesion to host tissues enhance cartilage regeneration, Bioact. Mater. 6 (2021) 1689–1698, https://doi.org/10.1016/j.bioactmat.2020.11.020.
[18] S. Bordbar, N. Lotfi Bakhshaiesh, M. Khanmohammadi, F.A. Sayahpour, M. Alini, M. Baghaban Eslaminejad, Production and evaluation of decellularized extracellular matrix hydrogel for cartilage regeneration derived from knee cartilage, J. Biomed. Mater. Res. 108 (2020) 938–946, https://doi.org/10.1002/jbm.a.36871.
[19] J. Zhu, S. Yang, Y. Qi, Z. Gong, H. Zhang, K. Liang, P. Shen, Y.-Y. Huang, Z. Zhang, W. Ye, L. Yue, S. Fan, S. Shen, A.G. Mikos, X. Wang, X. Fang, Stem cell–homing hydrogel-based miR-29b-5p delivery promotes cartilage regeneration by suppressing senescence in an osteoarthritis rat model, Sci. Adv. 8 (2022), https://doi.org/10.1126/sciadv.abk0011.
[20] B. Yang, J. Song, Y. Jiang, M. Li, J. Wei, J. Qin, W. Peng, F.L. Lasaosa, Y. He, H. Mao, J. Yang, Z. Gu, Injectable adhesive self-healing multicross-linked double-network hydrogel facilitates full-thickness skin wound healing, ACS Appl. Mater. Interfaces 12 (2020) 57782–57797, https://doi.org/10.1021/acsami.0c18948.
[21] T. Khodaei, J. Nourmohammadi, A. Ghaee, Z. Khodaii, An antibacterial and self-healing hydrogel from aldehyde-carrageenan for wound healing applications, Carbohydr. Polym. 302 (2023) 120371, https://doi.org/10.1016/j.carbpol.2022.120371.
[22] L. Mei, D. Zhang, H. Shao, Y. Hao, T. Zhang, W. Zheng, Y. Ji, P. Ling, Y. Lu, Q. Zhou, Injectable and self-healing probiotics-loaded hydrogel for promoting superbacteria-infected wound healing, ACS Appl. Mater. Interfaces 14 (2022) 20538–20550, https://doi.org/10.1021/acsami.1c23713.
[23] A.C. Hernández-González, L. Téllez-Jurado, L.M. Rodríguez-Lorenzo, Preparation of covalently bonded silica-alginate hybrid hydrogels by SCHIFF base and sol-gel reactions, Carbohydr. Polym. 267 (2021) 118186, https://doi.org/10.1016/j.carbpol.2021.118186.
[24] E. Yu, M. Zhang, G. Xu, X. Liu, J. Yan, Consensus cluster analysis of apoptosis-related genes in patients with osteoarthritis and their correlation with immune cell infiltration, Front. Immunol. 14 (2023), https://doi.org/10.3389/fimmu.2023.1202758.
[25] C.C. Pan, R. Maeso-Díaz, T.R. Lewis, K. Xiang, L. Tan, Y. Liang, L. Wang, F. Yang, T. Yin, C. Wang, K. Du, D. Huang, S.H. Oh, E. Wang, B.J.W. Lim, M. Chong, P. B. Alexander, X. Yao, V.Y. Arshavsky, Q.-J. Li, A.M. Diehl, X.-F. Wang, Antagonizing the irreversible thrombomodulin-initiated proteolytic signaling alleviates age-related liver fibrosis via senescent cell killing, Cell Res. 33 (2023) 516–532, https://doi.org/10.1038/s41422-023-00820-4.
[26] Z.-G. Sun, Yang-Liu, J.-M. Zhang, S.-C. Cui, Z.-G. Zhang, H.-L. Zhu, The research progress of direct thrombin inhibitors, Mini-Rev. Med. Chem. 20 (2020) 1574–1585, https://doi.org/10.2174/1389557519666191015201125.
[27] Q. Yao, X. Wu, C. Tao, W. Gong, M. Chen, M. Qu, Y. Zhong, T. He, S. Chen, G. Xiao, Osteoarthritis: pathogenic signaling pathways and therapeutic targets, Signal Transduct. Targeted Ther. 8 (2023) 56, https://doi.org/10.1038/s41392-023-01330-w.
[28] T. Szponder, M. Latalski, A. Danielewicz, K. Krać, A. Kozera, B. Drzewiecka, D. Nguyen Ngoc, D. Dobko, J. Wessely-Szponder, Osteoarthritis: pathogenesis, animal models, and new regenerative therapies, J. Clin. Med. 12 (2022) 5, https://doi.org/10.3390/jcm12010005.
[29] I. Onu, R. Gherghel, I. Nacu, F.-D. Cojocaru, L. Verestiuc, D.-V. Matei, D. Cascaval, I.L. Serban, D.A. Iordan, A. Tucaliuc, A.-I. Galaction, Can combining hyaluronic acid and physiotherapy in knee osteoarthritis improve the physicochemical properties of synovial fluid? Biomedicines 12 (2024) 449, https://doi.org/10.3390/biomedicines12020449.
[30] R.F. Loeser, S.R. Goldring, C.R. Scanzello, M.B. Goldring, Osteoarthritis: a disease of the joint as an organ, Arthritis Rheum. 64 (2012) 1697–1707, https://doi.org/10.1002/art.34453.
[31] L.W. Moreland, Intra-articular hyaluronan (hyaluronic acid) and hylans for the treatment of osteoarthritis: mechanisms of action, Arthritis Res. Ther. 5 (2003) 54, https://doi.org/10.1186/ar623.
[32] X. Xue, Y. Hu, S. Wang, X. Chen, Y. Jiang, J. Su, Fabrication of physical and chemical crosslinked hydrogels for bone tissue engineering, Bioact. Mater. 12 (2022) 327–339, https://doi.org/10.1016/j.bioactmat.2021.10.029.
[33] Y. Lei, X. Wang, J. Liao, J. Shen, Y. Li, Z. Cai, N. Hu, X. Luo, W. Cui, W. Huang, Shear-responsive boundary-lubricated hydrogels attenuate osteoarthritis, Bioact. Mater. 16 (2022) 472–484, https://doi.org/10.1016/j.bioactmat.2022.02.016.
[34] A.R. Martin, J.M. Patel, R.C. Locke, M.R. Eby, K.S. Saleh, M.D. Davidson, M. L. Sennett, H.M. Zlotnick, A.H. Chang, J.L. Carey, J.A. Burdick, R.L. Mauck, Nanofibrous hyaluronic acid scaffolds delivering TGF-β3 and SDF-1α for articular cartilage repair in a large animal model, Acta Biomater. 126 (2021) 170–182, https://doi.org/10.1016/j.actbio.2021.03.013.
[35] N. Gerwin, C. Hops, A. Lucke, Intraarticular drug delivery in osteoarthritis, Adv. Drug Deliv. Rev. 58 (2006) 226–242, https://doi.org/10.1016/j.addr.2006.01.018.
[36] F. Xiong, Z. Qin, H. Chen, Q. Lan, Z. Wang, N. Lan, Y. Yang, L. Zheng, J. Zhao, D. Kai, pH-responsive and hyaluronic acid-functionalized metal–organic frameworks for therapy of osteoarthritis, J. Nanobiotechnol. 18 (2020) 139, https://doi.org/10.1186/s12951-020-00694-3.
[37] L. Lei, R. Cong, Y. Ni, X. Cui, X. Wang, H. Ren, Z. Wang, M. Liu, J. Tu, L. Jiang, Dual-functional injectable hydrogel for osteoarthritis treatments, Adv. Healthcare Mater. 13 (2024), https://doi.org/10.1002/adhm.202302551.
[38] Q. Li, S. Miramini, D.W. Smith, B.S. Gardiner, L. Zhang, Osteochondral junction leakage and cartilage joint lubrication, Comput. Methods Progr. Biomed. 230 (2023) 107353, https://doi.org/10.1016/j.cmpb.2023.107353.

[39] S. Jahn, J. Seror, J. Klein, Lubrication of articular cartilage, Annu. Rev. Biomed. Eng. 18 (2016) 235–258, https://doi.org/10.1146/annurev-bioeng-081514-123305.
[40] H. Qiu, J. Deng, R. Wei, X. Wu, S. Chen, Y. Yang, C. Gong, L. Cui, Z. Si, Y. Zhu, R. Wang, D. Xiong, A lubricant and adhesive hydrogel cross-linked from hyaluronic acid and chitosan for articular cartilage regeneration, Int. J. Biol. Macromol. 243 (2023) 125249, https://doi.org/10.1016/j.ijbiomac.2023.125249.
[41] Y. Lei, Y. Wang, J. Shen, Z. Cai, C. Zhao, H. Chen, X. Luo, N. Hu, W. Cui, W. Huang, Injectable hydrogel microspheres with self-renewable hydration layers alleviate osteoarthritis, Sci. Adv. 8 (2022), https://doi.org/10.1126/sciadv.abl6449.
[42] S. Scheiner, Understanding noncovalent bonds and their controlling forces, J. Chem. Phys. 153 (2020), https://doi.org/10.1063/5.0026168.
[43] P. du Souich, Absorption, distribution and mechanism of action of SYSADOAS, Pharmacol. Ther. 142 (2014) 362–374, https://doi.org/10.1016/j.pharmthera.2014.01.002.
[44] A. Fakhari, C. Berkland, Applications and emerging trends of hyaluronic acid in tissue engineering, as a dermal filler and in osteoarthritis treatment, Acta Biomater. 9 (2013) 7081–7092, https://doi.org/10.1016/j.actbio.2013.03.005.
[45] O. Ishida, Y. Tanaka, I. Morimoto, M. Takigawa, S. Eto, Chondrocytes are regulated by cellular adhesion through CD44 and hyaluronic acid pathway, J. Bone Miner. Res. 12 (1997) 1657–1663, https://doi.org/10.1359/jbmr.1997.12.10.1657.
[46] S. Amorim, C.A. Reis, R.L. Reis, R.A. Pires, Extracellular matrix mimics using hyaluronan-based biomaterials, Trends Biotechnol. 39 (2021) 90–104, https://doi.org/10.1016/j.tibtech.2020.06.003.
[47] D. Zhou, S. Li, M. Pei, H. Yang, S. Gu, Y. Tao, D. Ye, Y. Zhou, W. Xu, P. Xiao, Dopamine-modified hyaluronic acid hydrogel adhesives with fast-forming and high tissue adhesion, ACS Appl. Mater. Interfaces 12 (2020) 18225–18234, https://doi.org/10.1021/acsami.9b22120.
[48] Z. Tang, F. Jiang, Y. Zhang, Y. Zhang, YuanYang, X. Huang, Y. Wang, D. Zhang, N. Ni, F. Liu, M. Luo, X. Fan, W. Zhang, P. Gu, Mussel-inspired injectable hydrogel and its counterpart for actuating proliferation and neuronal differentiation of retinal progenitor cells, Biomaterials 194 (2019) 57–72, https://doi.org/10.1016/j.biomaterials.2018.12.015.
[49] A.I. Neto, A.C. Cibrão, C.R. Correia, R.R. Carvalho, G.M. Luz, G.G. Ferrer, G. Botelho, C. Picart, N.M. Alves, J.F. Mano, Nanostructured polymeric coatings based on chitosan and dopamine-modified hyaluronic acid for biomedical applications, Small 10 (2014) 2459–2469, https://doi.org/10.1002/smll.201303568.
[50] K.N. Antonas, J.R. Fraser, K.D. Muirden, Distribution of biologically labelled radioactive hyaluronic acid injected into joints, Ann. Rheum. Dis. 32 (1973) 103–111, https://doi.org/10.1136/ard.32.2.103.
[51] K.S.M. Reed, V. Ulici, C. Kim, S. Chubinskaya, R.F. Loeser, D.H. Phanstiel, Transcriptional response of human articular chondrocytes treated with fibronectin fragments: an in vitro model of the osteoarthritis phenotype, Osteoarthritis Cartilage 29 (2021) 235–247, https://doi.org/10.1016/j.joca.2020.09.006.
[52] T. Yasuda, Activation of Akt leading to NF-κB up-regulation in chondrocytes stimulated with fibronectin fragment, Biomed. Res. 32 (2011) 209–215, https://doi.org/10.2220/biomedres.32.209.
[53] G.M. Campo, A. Avenoso, A. D'Ascola, M. Scuruchi, V. Prestipino, A. Calatroni, S. Campo, Hyaluronan in part mediates IL-1beta-induced inflammation in mouse chondrocytes by up-regulating CD44 receptors, Gene 494 (2012) 24–35, https://doi.org/10.1016/j.gene.2011.11.064.
[54] L.-J. Kang, J. Yoon, J.G. Rho, H.S. Han, S. Lee, Y.S. Oh, H. Kim, E. Kim, S.J. Kim, Y. T. Lim, J.H. Park, W.K. Song, S. Yang, W. Kim, Self-assembled hyaluronic acid nanoparticles for osteoarthritis treatment, Biomaterials 275 (2021) 120967, https://doi.org/10.1016/j.biomaterials.2021.120967.
[55] H. Chen, F. Fei, X. Li, Z. Nie, D. Zhou, L. Liu, J. Zhang, H. Zhang, Z. Fei, T. Xu, A structure-supporting, self-healing, and high permeating hydrogel bioink for establishment of diverse homogeneous tissue-like constructs, Bioact. Mater. 6 (2021) 3580–3595, https://doi.org/10.1016/j.bioactmat.2021.03.019.
[56] T. Son, M. Kim, M. Choi, S.H. Nam, A. Yoo, H. Lee, E.H. Han, K.S. Hong, H.S. Park, Advancing fluorescence imaging: enhanced control of cyanine dye-doped silica nanoparticles, J. Nanobiotechnol. 22 (2024) 347, https://doi.org/10.1186/s12951-024-02638-7.
[57] D. Kang, J. Shin, Y. Cho, H.-S. Kim, Y.-R. Gu, H. Kim, K.T. You, M.J. Chang, C. B. Chang, S.-B. Kang, J.-S. Kim, V.N. Kim, J.-H. Kim, Stress-activated miR-204 governs senescent phenotypes of chondrocytes to promote osteoarthritis development, Sci. Transl. Med. 11 (2019), https://doi.org/10.1126/scitranslmed.aar6659.